



Modeling biogeochemical processes in subterranean estuaries: Effect of flow dynamics and redox conditions on submarine groundwater discharge of nutrients

Claudette Spiteri,¹ Caroline P. Slomp,¹ Kagan Tuncay,² and Christof Meile³

Received 29 March 2007; revised 28 August 2007; accepted 18 September 2007; published 22 February 2008.

[1] A two-dimensional density-dependent reactive transport model, which couples groundwater flow and biogeochemical reactions, is used to investigate the fate of nutrients (NO_3^- , NH_4^+ , and PO_4) in idealized subterranean estuaries representing four end-members of oxic/anoxic aquifer and seawater redox conditions. Results from the simplified model representations show that the prevalent flow characteristics and redox conditions in the freshwater-seawater mixing zone determine the extent of nutrient removal and the input of nitrogen and phosphorus to coastal waters. At low to moderate groundwater velocities, simultaneous nitrification and denitrification can lead to a reversal in the depth of freshwater NO_3^- and NH_4^+ - PO_4 plumes, compared to their original positions at the landward source. Model results suggest that autotrophic denitrification pathways with Fe^{2+} or FeS_2 may provide an important, often overlooked link between nitrogen and phosphorus biogeochemistry through the precipitation of iron oxides and subsequent binding of phosphorus. Simulations also highlight that deviations of nutrient data from conservative mixing curves do not necessarily indicate nutrient removal.

Citation: Spiteri, C., C. P. Slomp, K. Tuncay, and C. Meile (2008), Modeling biogeochemical processes in subterranean estuaries: Effect of flow dynamics and redox conditions on submarine groundwater discharge of nutrients, *Water Resour. Res.*, 44, W02430, doi:10.1029/2007WR006071.

1. Introduction

[2] The discharge of groundwater into nearshore marine environments, often termed submarine groundwater discharge (SGD), is an important transport pathway for a variety of dissolved chemical species such as nutrients, metals, radionuclides and organic compounds [Burnett *et al.*, 2006; Charette and Sholkovitz, 2006; Paytan *et al.*, 2006; Windom *et al.*, 2006]. The *Scientific Committee on Oceanic Research* [2004] gives an annual global estimate of freshwater SGD of 2400 km³, which makes up ~6% of the world's river discharge, whereas previous estimates of global SGD vary between 0.01 to 10% of surface runoff [Church, 1996]. There is also a wide variation in the reported worldwide SGD rates, which range from 0.03 to 454 m a⁻¹ (where a is years), most of which fall below 36 m a⁻¹ and may consist of both freshwater and recirculated seawater [Taniguchi *et al.*, 2002]. Especially in areas strongly influenced by human activities, freshwater SGD may contain high concentrations of nutrients and can significantly contribute “new” nutrients to the coastal zone [e.g., Capone and Bautista, 1985; Slomp and Van Cappellen, 2004]. For example, in a field study of the seasonal groundwater contribution to the nutrient budget of

Tomales Bay, California [Oberdorfer *et al.*, 1990], the dissolved nutrient concentrations in groundwater were consistently an order of magnitude higher than values in surface water discharge. Johannes [1980] also observed that the nitrate (NO_3^-) levels in SGD in the Perth area, Australia, were significantly higher than in surface runoff, with a conservative ratio estimate of 3:1. Note, however, that in areas with low freshwater discharge rates, recirculated seawater is often the major component of SGD and may contribute to coastal recycling of nutrients [Burnett *et al.*, 2007]. Overall, groundwater concentrations of nutrients in various parts of the world are often 2–3 orders of magnitude greater than concentrations in typical coastal waters [Slomp and Van Cappellen, 2004]. Therefore, even if SGD rates may be lower than surface runoff, groundwater may still constitute an important source of NO_3^- to the coastal zone.

[3] The discharge of groundwater contaminated with both nitrogen (N) and phosphorus (P), for example, originating from fertilizer/manure leachates and wastewater from septic systems, can lead to changes in the structure and function of shallow coastal ecosystems [e.g., Johannes, 1980]. As a result of P adsorption onto iron- and aluminum-oxides in soils, sediments, aquifers and coastal sands [Krom and Berner, 1980; Frossard *et al.*, 1995; Spiteri *et al.*, 2006], P loading through freshwater SGD is typically well attenuated [Sewell, 1982; Johannes and Hearn, 1985]. This may alter the dissolved inorganic nitrogen to phosphorus (N:P) ratios of SGD, trigger eutrophication in N-limited coastal waters [Howarth, 1988] and promote the growth of algal blooms [Sewell, 1982; LaRoche *et al.*, 1990; Paerl, 1997]. Ultimately, freshwater SGD with N:P ratios higher than the

¹Department of Earth Science–Geochemistry, Faculty of Geosciences, Utrecht University, Utrecht, Netherlands.

²Faculty of Engineering, Middle East Technical University, Ankara, Turkey.

³Department of Marine Sciences, University of Georgia, Athens, Georgia, USA.

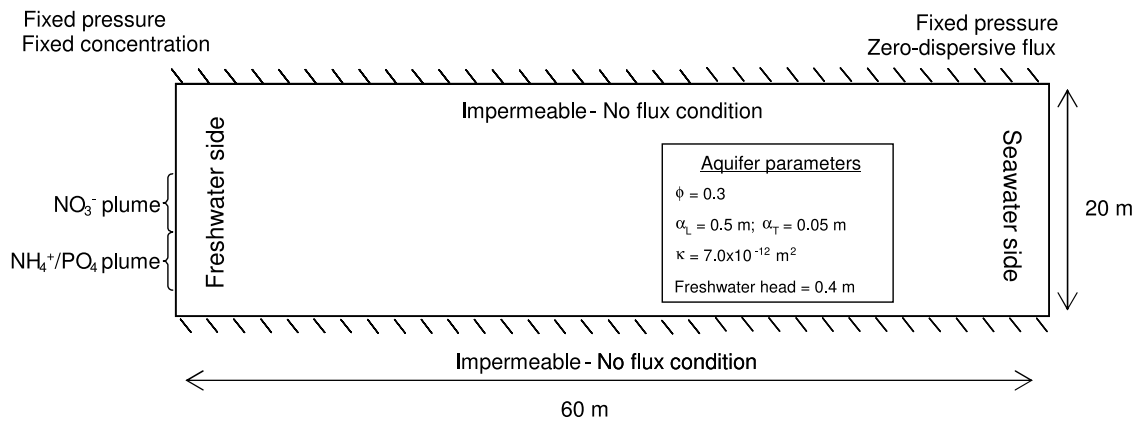


Figure 1. Schematic diagram of the model setup, showing the model domain, boundary conditions, aquifer parameters (ϕ is porosity; α_L is longitudinal dispersivity; α_T is transverse dispersivity; and κ is permeability), and the depths of the nutrient source plumes. The freshwater head of 0.4 m imposed at the landward boundary in the baseline simulations results in a hydraulic gradient of 0.0067 m m^{-1} .

requirements of phytoplankton may drive coastal production toward P limitation [Slomp and Van Cappellen, 2004].

[4] Most studies to date have focused on the identification of hot spots for SGD and quantification of SGD rates [Cable et al., 1996; Corbett et al., 1999; Crusius et al., 2005; Burnett et al., 2006]. Groundwater-derived nutrient fluxes are commonly estimated (1) by multiplying SGD rates or inland groundwater flow rates with the average nutrient concentrations in groundwater [Lapointe et al., 1990; Oberdorfer et al., 1990; Giblin and Gaines, 1990; Boehm et al., 2006; Swarzenski et al., 2006], (2) by using mass balance calculations/nutrient budgets [Valiela et al., 1990; Weiskel and Howes, 1992] or (3) by applying loading models based on empirical relationships [Weiskel and Howes, 1991; Valiela et al., 1997], particularly in catchment-scale studies. All three approaches used for the quantification of coastal nutrient fluxes are subject to assumptions and large uncertainties. For example, groundwater flow rates can fluctuate spatially as well as temporally, and nutrient concentrations in groundwater can vary spatially by several orders of magnitude [Giblin and Gaines, 1990]. Thus the determination of nutrient fluxes from point measurements might not always be representative. Flux estimates based on loading models also require many assumptions on the subsurface transport, human occupancy, initial loading rates and transport behavior [Weiskel and Howes, 1991], all of which could lead to substantial uncertainties in SGD estimates.

[5] As pointed out by Giblin and Gaines [1990] and Slomp and Van Cappellen [2004], the chemical composition of SGD is not only affected by the landward freshwater sources and discharge rates, but also by the reactions within the subterranean estuaries, the mixing zone of freshwater and seawater in coastal aquifers [Moore, 1999]. Nutrient dynamics in these coastal mixing zones, and hence SGD of nutrients, are strongly influenced by the redox characteristics of the freshwater and seawater end-members [Capone and Slater, 1990; Uchiyama et al., 2000; Charette and Sholkovitz, 2002; Ueda et al., 2003; Nyvang, 2003]. Nonetheless, in many field studies of SGD, this nearshore removal and transformation of nutrients is not accounted for.

[6] In this study, we quantify nutrient (NO_3^- , NH_4^+ , PO_4) inputs to the coastal ocean through SGD, accounting for the

redox-dependent transformation and removal processes that occur prior to discharge using reactive transport modeling. In a recent review, Slomp and Van Cappellen [2004] discussed the effect of the prevailing biogeochemical reactions on the discharge of N and P for four redox end-member settings: case 1, oxic groundwater meeting oxic seawater; case 2, oxic groundwater meeting anoxic seawater; case 3, anoxic groundwater meeting oxic seawater; and case 4, anoxic groundwater meeting anoxic seawater.

[7] We adopt this classification to assess the relevance of the processes postulated in their conceptual models and to study the key factors controlling nutrient loadings to coastal areas, using a two-dimensional (2-D) density-dependent, process-based reactive transport model. The main aims of this study are (1) to identify those processes and conditions relevant for the mitigation of N and P prior to SGD and (2) to quantify their respective fluxes into the coastal ocean in the four end-member settings. The fresh groundwater is assumed to be contaminated with shallow NO_3^- and $\text{NH}_4^+ - \text{PO}_4$ plumes, which typically originate from sewage effluents along the coast. We first perform four baseline simulations to assess the impact of prevalent redox conditions on nutrient distributions in the aquifer, nutrient fluxes and the resulting N:P ratios of SGD. Then we perform a sensitivity analysis to assess the role of specific aquifer parameters, such as transverse dispersivity (α_T), and additional reactions on the nutrient biogeochemistry in coastal aquifers. The latter include denitrification with Fe^{2+} and pyrite as electron donors, removal of PO_4 through hydroxyapatite precipitation, as well as an investigation of the interplay between flow rates and dissolved organic matter (DOM) reactivity on NO_3^- production/removal through nitrification/denitrification.

2. Model Setup

[8] A schematic diagram of the rectangular model domain, representing a typical shallow coastal aquifer system, and the corresponding aquifer parameters are given in Figure 1. A uniform grid ($\Delta x = 0.6 \text{ m}$; $\Delta z = 0.33 \text{ m}$) is used for the discretization of the model domain, resulting in a total of 6000 elements. The time step is fixed at 6480 seconds. The imposed fresh groundwater head (Figure 1) ensures that the steady state saltwater wedge

Table 1. Concentrations of the Different Species Assumed in the Four Water Types^a

Species ^b	Concentration in Oxidic Groundwater	Concentration in Anoxic Groundwater	Concentration in Oxidic Seawater	Concentration in Anoxic Seawater
Salinity	0.28 (1)	0.28 (1)	27.0 (1)	27.0 (1)
NO ₃ ⁻	0.25 (2) ^c	0.25 (2) ^c	0.02 (3)	-
NH ₄ ⁺	-	0.2 (4) ^c	-	0.01 (4)
PO ₄	0.001 (2) ^c	0.05 (2) ^c	0.001 (3)	0.3 (4)
PO ₄ (ads) (s)	-	-	-	-
O ₂	0.05 (2)	0.0	0.2 (3)	0.0
DOM	-	0.75 (4)	-	0.33 (4)
Fe ²⁺	-	0.1 (1)	-	0.1 (1)
Fe(OH) ₃ (s) ^d	-	-	-	-
FeS ₂ (s) ^d	NA	25.0 (5)	25.0 (5)	25.0 (5)
Ca ²⁺	-	1.0 (4)	10.5 (3)	6.7 (4)
Ca ₅ (PO ₄) ₃ OH (s)	-	-	-	-
N:P ratio ^e	250	9	-	-

^aSources within parentheses are as follows: 1, *Charette et al.* [2005]; 2, *Slomp and Van Cappellen* [2004]; 3, *Berner and Berner* [1996]; 4, *Nyvang* [2003]; 5, equivalent to 10 mmol kg⁻¹ [*Appelo and Postma*, 2005]. Dash indicates low concentrations, assumed to be 0; NA is not available.

^bUnits for solutes are in mmol dm⁻³ pore water, denoted as mM; solids (s) are in mmol dm⁻³ solid, denoted as mmol dm⁻³; units for salinity are per mil.

^cThese are anthropogenic plumes; NO₃⁻ plume is at 8–12 m depth; NH₄⁺/PO₄ plumes co-occur at 12–16 m depth; background concentrations are set to 0.

^dFe(OH)₃ is formed “in situ” at the redox boundary, whereas pyrite is assumed to be uniformly present throughout the whole domain.

^eNote that the computed N:P ratios as the freshwater sources assume the spatial overlapping of the (NO₃⁻ + NH₄⁺) and PO₄ plumes.

does not interfere with the landward boundary. The solute chemical constituents included in the model are salinity, NO₃⁻, NH₄⁺, PO₄, Ca²⁺, DOM, Fe²⁺ and O₂, while Ca₅(PO₄)₃OH, Fe(OH)₃, FeS₂ and adsorbed P (PO₄(ads)) are solid species. Table 1 provides the concentrations in the different parts of the aquifers assumed in the four cases. Oxidic and anoxic groundwater is impacted by a NO₃⁻ plume, which is presumably produced as the groundwater travels through the predominantly oxidic unsaturated zone, while an NH₄⁺ plume is only present in anoxic groundwater (cases 3 and 4). A PO₄ plume is considered in all cases, but with a much lower concentration in the oxidic groundwater, owing to the presumably extensive removal in the unsaturated zone through sorption (cases 1 and 2).

[9] The reaction network, comprised of 9 kinetic reactions, and the corresponding reaction parameters are given in Tables 2 and 3, respectively. DOM degradation (Table 2) proceeds from aerobic respiration to denitrification to Fe(OH)₃ reduction, assuming a first-order rate with respect to the electron donor, DOM, and a linearized Monod dependency on the electron acceptor. Pyrite oxidation with O₂ and denitrification with pyrite follow a similar stepwise inhibition sequence used for DOM degradation, with a first-order dependency on O₂ and NO₃⁻, respectively [*Wriedt and Rode*, 2006]. Nitrification and Fe²⁺ oxidation with O₂ and NO₃⁻ are described by bimolecular rate laws. The removal of P through adsorption of dissolved PO₄ is included as the instantaneous redistribution of total PO₄ into dissolved and adsorbed P. Sorption is represented by a sorption isotherm, in which the adsorption coefficient (K_d) is a function of the concentration of Fe(OH)₃ (Table 2). The rate of hydroxyapatite (Ca₅(PO₄)₃OH) precipitation depends on the degree of mineral undersaturation or supersaturation of the groundwater (Table 2), following the formulation of *Spiteri et al.* [2007a]. The current model does not explicitly account for the production/consumption of protons (Table 2) and for the effect of pH on particular reaction kinetics. Moreover, the nonlinear effects of pH in the freshwater-seawater mixing zone [e.g., *Wigley and Plummer*, 1976] are not considered.

[10] Model calculations are performed for a saturated porous medium, using the classical Darcy flow approximation. In each time step, the pressure field is first calculated, taking into account density variations as a linear function of salinity. From the calculated pressure field, the velocity field is derived using the Darcy law, and the anisotropic dispersion tensor is obtained for the given longitudinal and transverse dispersivities (α_L , α_T , respectively [*Scheidegger*, 1961]). Concentration fields are then computed by solving the equations for conservation of mass for all species, considering diffusive/dispersible and advective transport for solutes. We use a Galerkin finite element formulation for spatial discretization and a conjugate gradient approach to solve the linear set of equations at each time step [*Reddy*, 1993; *Meile and Tuncay*, 2006]. Details of the mathematical model are provided in the appendix.

[11] In the model, we impose an impermeable (no flux) boundary condition at the top and bottom boundaries (Figure 1). The lower boundary represents a delimiting confining layer, while recharge at the water table is assumed negligible. Pressure is imposed on both the freshwater and seawater sides. The concentration at the freshwater side is fixed for all species, whereas at the seawater side, seawater is allowed to enter the domain through advection. The effect of tidal pumping and seasonal variation in freshwater discharge are not taken into account. The boundary conditions and initial concentrations are given in Figure 1 and Table 1, respectively. Our model setup depicts a subterranean estuary with representative fluid compositions and domain-scale aquifer characteristics, but does not account for any geological and hydrological heterogeneities.

3. Results and Discussion

3.1. Baseline Simulations

3.1.1. Flow Dynamics

[12] The modeled velocity field and corresponding salt wedge which penetrates a landward distance of 45 m at steady state are shown in Figures 2a and 2b, respectively. The groundwater discharge into the sea, composed of freshwater and recirculated seawater SGD, is characterized

Table 2. Reaction Network and Kinetic Formulations Used in the Model

Name	Reaction ^a	Kinetic Formulation ^a
Oxic degradation	$(CH_2O)_x (NH_3)_y (H_3PO_4)_z + x \cdot O_2 + (-y + 2z) HCO_3^-$ $\rightarrow (x - y + 2z) CO_2 + yNH_4^+ + zHPO_4^{2-} + (x - y + 2z) H_2O$	<p><i>Reaction Network Used in "Base Simulations"</i></p> <p>If $O_2 > kmo2$; rate = $k_{fox} [(CH_2O)_x (NH_3)_y (H_3PO_4)_z] \cdot \frac{[O_2]}{[kmo2]}$</p> <p>If $O_2 < kmo2$; rate = $k_{fox} [(CH_2O)_x (NH_3)_y (H_3PO_4)_z] \cdot \left(1 - \frac{[O_2]}{[kmo2]}\right)$</p> <p>If $O_2 < kmo2$ and $NO_3^- > kmno3$; rate = $k_{fox} [(CH_2O)_x (NH_3)_y (H_3PO_4)_z] \cdot \left(1 - \frac{[O_2]}{[kmo2]}\right) \cdot \frac{[NO_3^-]}{[kmno3]}$</p>
Denitrification	$(CH_2O)_x (NH_3)_y (H_3PO_4)_z + 0.8x \cdot NO_3^-$ $\rightarrow 0.4x \cdot N_2 + (0.2x - y + 2z) CO_2 + (0.8x + y - 2z) HCO_3^-$ $+ yNH_4^+ + zHPO_4^{2-} + (0.6x - y + 2z) H_2O$	<p>If $NO_3^- < kmno3$ and $NO_3^- < kmno3$; rate = $k_{fox} [(CH_2O)_x (NH_3)_y (H_3PO_4)_z] \cdot \left(1 - \frac{[O_2]}{[kmo2]}\right) \cdot \frac{[NO_3^-]}{[kmno3]}$</p> <p>If $NO_3^- > kmno3$; rate = 0.</p> <p>If $NO_3^- < kmno3$ and $Fe(OH)_3 > kmfe$; rate = $k_{fox} [(CH_2O)_x (NH_3)_y (H_3PO_4)_z] \cdot \left(1 - \frac{[O_2]}{[kmo2]}\right) \cdot \frac{[NO_3^-]}{[kmno3]}$</p>
Fe(OH) ₃ reduction	$(CH_2O)_x (NH_3)_y (H_3PO_4)_z + 4x \cdot Fe(OH)_3 + (7x + y - 2z) CO_2$ $\rightarrow 4x \cdot Fe^{2+} + (8x + y - 2z) HCO_3^- + yNH_4^+ + zHPO_4^{2-}$ $+ (3x - y + 2z) H_2O$	<p>If $NO_3^- < kmno3$ and $Fe(OH)_3 < kmfe$; rate = $k_{fox} [(CH_2O)_x (NH_3)_y (H_3PO_4)_z] \cdot \left(1 - \frac{[O_2]}{[kmo2]}\right) \cdot \frac{[Fe(OH)_3]}{[kmfe]}$</p> <p>Rate = $k_{init} [NH_4^+] [O_2]$</p> <p>Rate = $k_{fox} [Fe^{2+}] [O_2]$</p>
Nitrification	$NH_4^+ + 2O_2 + 2HCO_3^- \rightarrow NO_3^- + 2CO_2 + 3H_2O$	
Fe ²⁺ reoxidation	$Fe^{2+} + 0.25O_2 + 2HCO_3^- + 0.5H_2O \rightarrow Fe(OH)_3 + 2CO_2$	
PO ₄ adsorption ^b	$K_d \cdot \frac{\rho}{1 - \rho} = \frac{[PO_4(ads)]}{[PO_4]}$	
Denitrification via Fe ²⁺	$5Fe^{2+} + NO_3^- + 12H_2O \rightarrow 5Fe(OH)_3 + 0.5N_2 + 9H^+$	
Pyrite oxidation	$FeS_2 + 3.5O_2 + H_2O \rightarrow Fe^{2+} + 2SO_4^{2-} + 2H^+$	
Pyrite denitrification	$FeS_2 + 2.8NO_3^- + 0.8H^+$ $\rightarrow Fe^{2+} + 2SO_4^{2-} + 1.4N_2 + 0.4H_2O$	<p><i>Extended Reaction Network Used in "Sensitivity Analysis"</i></p> <p>Rate = $k_{denit} [Fe^{2+}] [NO_3^-]$</p> <p>If $O_2 > kmo2$; rate = $k_{pyox} \frac{[O_2]}{[kmo2]}$</p> <p>If $O_2 < kmo2$; rate = $k_{pyox} \frac{[O_2]}{[kmo2]}$</p> <p>If $O_2 > kmo2$ and $NO_3^- > kmno3$; rate = 0.</p> <p>If $O_2 < kmo2$ and $NO_3^- > kmno3$; rate = $k_{pydenit} [NO_3^-] \cdot \left(1 - \frac{[O_2]}{[kmo2]}\right) \cdot \frac{[NO_3^-]}{[kmno3]}$</p>
Hydroxyapatite precipitation	$5Ca^{2+} + 3HPO_4^{2-} + H_2O \rightarrow Ca_5(PO_4)_3(OH) + 4H^+$	<p>If $O_2 < kmo2$ and $NO_3^- < kmno3$; rate = $k_{ppdenit} [NO_3^-] \cdot \left(1 - \frac{[O_2]}{[kmo2]}\right) \cdot \frac{[NO_3^-]}{[kmno3]}$</p> <p>Rate = $k_{HA} (\Omega_{HA} - 1)^c$</p>

^aHere x, y, and z represent the C:N:P ratios set as 106:1:1 for coastal environments [Van Cappellen and Wang, 1995].

^bThis is not a kinetic reaction but an instantaneous redistribution of PO_{4(ads)} into PO₄ and PO_{4(ads)}. K_d = K * Fe(OH)₃.

^c $\Omega_{HA} = \frac{[Ca^{2+}]^5 \cdot [HPO_4^{2-}]^3}{[H^+]^4 \cdot K_{HA}}$, where rate = 0 if $\Omega_{HA} < 1$. For salinity <25‰, pH = 7.0; for salinity >25‰, pH = 8.2.

Table 3. Reaction Parameter Values Used in the Model

Parameter	Description	Value
k_{fox} , s^{-1}	rate constant for decomposition of DOM	$3.0 \times 10^{-9\text{a}}$
k_{nitr} , $\text{mM}^{-1} \text{s}^{-1}$	rate constant for nitrification	$4.8 \times 10^{-4\text{a}}$
k_{feox} , $\text{mM}^{-1} \text{s}^{-1}$	rate constant for Fe^{2+} reoxidation	$6.4 \times 10^{-2\text{a}}$
k_{mo2} , mM	limiting concentration of O_2	0.008^{a}
k_{mno3} , mM	limiting concentration of NO_3^-	0.001^{a}
k_{mfe} , mM	limiting concentration of $\text{Fe}(\text{OH})_3$	18.95^{a}
k_{feno3} , $\text{mM}^{-1} \text{s}^{-1}$	rate constant for Fe^{2+} denitrification	$6.4 \times 10^{-2\text{b}}$
k_{pyox} , s^{-1}	first-order rate constant for pyrite oxidation	$3.7 \times 10^{-7\text{c}}$
k_{pydenit} , s^{-1}	first-order rate constant for pyrite denitrification	$2.2 \times 10^{-8\text{d}}$
K_{HA} (-)	solubility product for $\text{Ca}_5(\text{PO}_4)_3(\text{OH})$	$3.8 \times 10^{-4\text{e}}$
k_{HA} , $\text{mmol dm}^{-3} \text{s}^{-1}$	rate constant for $\text{Ca}_5(\text{PO}_4)_3(\text{OH})$ precipitation	$2.3 \times 10^{-15\text{f}}$
K , $\text{dm}^3 \text{mmol}^{-1}$	adsorption coefficient for PO_4	1545^{g}

^aVan Cappellen and Wang [1995].

^bAssumed to be equal to the value for Fe^{2+} reoxidation with O_2 .

^cKamei and Ohmoto [2000].

^dFrind et al. [1990].

^ePHREEQE database.

^fInskip and Silvertooth [1988].

^gCalculated assuming a $\text{Fe}(\text{OH})_3$ concentration of 0.2 mmol dm^{-3} and a dimensionless K_4 of 309 [Krom and Berner, 1980].

by positive velocities, implying outflow in the sea. Because of the constriction of the groundwater flow into a narrow zone, as illustrated by the converging velocity vectors in Figure 2a, the maximum linear horizontal velocities reach as high as 100 m a^{-1} , contrasting with a velocity of $\sim 2 \text{ m a}^{-1}$ for the inflowing seawater (Figure 2c). The salinity profile at the seaward boundary (Figure 2d) shows a sharp interface

between SGD and the inflowing seawater at a depth of $\sim 4.5 \text{ m}$.

3.1.2. Nutrient Distributions

[13] Modeled steady state concentration distributions of NO_3^- , NH_4^+ and PO_4 for cases 1–4 are shown in Figure 3. A set of analogous simulations are also performed in which all reactions are turned off, referred to as “conservative” runs.

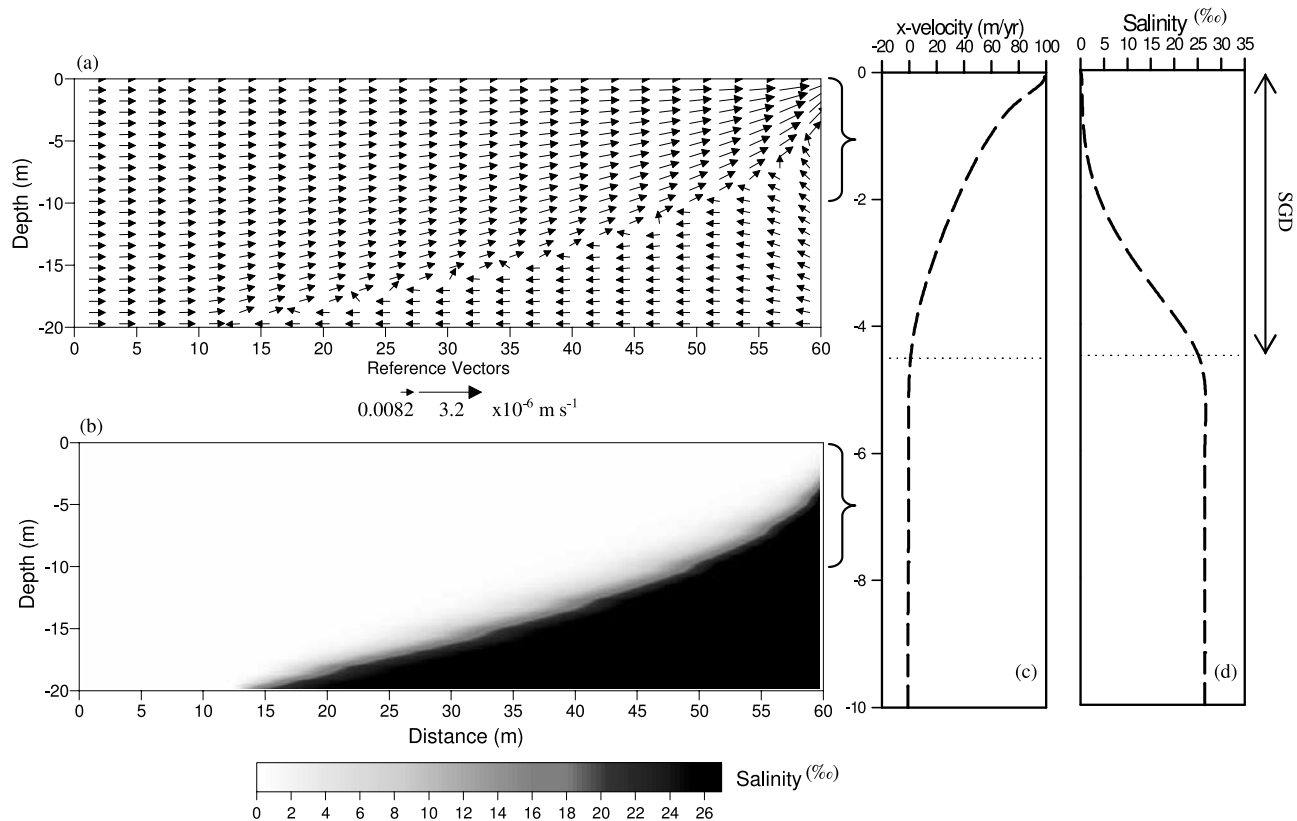


Figure 2. (a) Resultant velocity vector field and (b) steady state Ghyben-Herzberg type salt wedge formed in the model coastal aquifer. (c) The x velocity profile over the top 10 m depth at the seaward boundary, where the average SGD rate of $\sim 50 \text{ m a}^{-1}$ falls within the worldwide range of $0.03\text{--}454 \text{ m a}^{-1}$ [Taniguchi et al., 2002]. (d) Salinity profile over the top 10 m depth at the seaward boundary. The horizontal dotted lines in Figures 2c and 2d indicate the (freshwater and recirculated seawater)-seawater interface, based on the x velocity profile in Figure 2c.

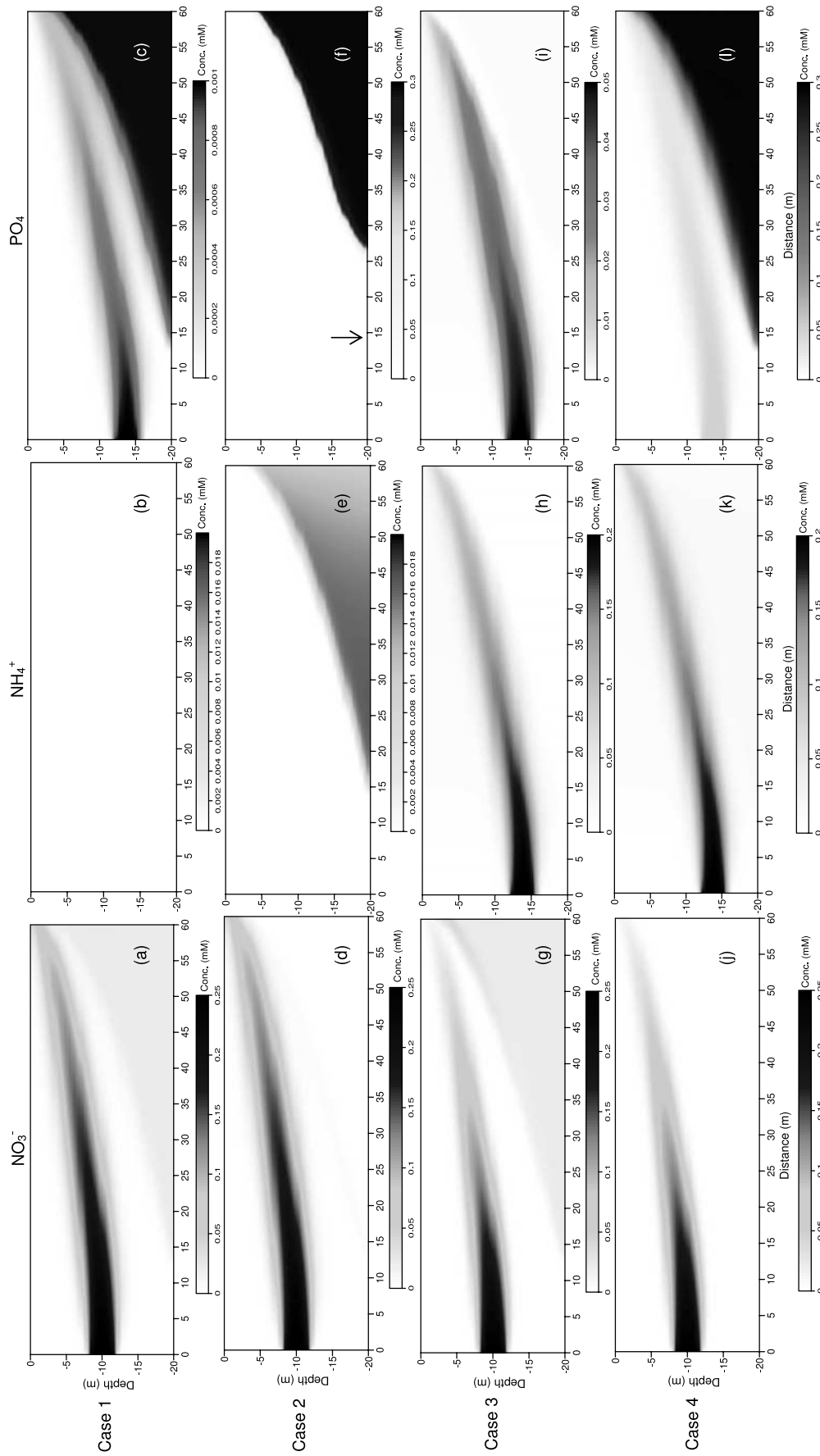


Figure 3

For comparison, Figure 4 shows the steady state concentration profiles of the most important solute species at the seaward boundary, plotted together with the respective “conservative” profiles.

[14] In case 1, the N and P species in the completely oxic model subterranean estuary show very limited transformation or removal (Figures 4a–4e), because of the absence of reactive DOM (Table 1). The seaward conservative propagation of the NO_3^- plume follows a tangential flow path, bending upward over the saltwater wedge, owing to the density variations between the freshwater and seawater. A significant drop in the peak discharge concentration of both NO_3^- and PO_4 , relative to the source concentrations, is observed as a result of dispersion/dilution (Figures 3a and 3c). In general, NO_3^- is expected to be the predominant nutrient in oxic subterranean estuaries.

[15] The interaction of oxic groundwater with anoxic seawater in case 2 affects the NH_4^+ profile at the seaward boundary (Figure 4g). Nitrification lowers the NH_4^+ concentrations in the freshwater part, whereas NH_4^+ concentration increases (from 0.01 to ~ 0.02 mM; Figure 3e) in the seawater wedge because of DOM degradation. The NH_4^+ transported in the anoxic seawater is nitrified to NO_3^- as it meets the O_2 in the oxic groundwater, slightly increasing the NO_3^- concentrations along the interface (Figure 4f). The net removal of NO_3^- from the entire model domain is only marginal, mainly because denitrification is hindered by the presence of O_2 in the oxic groundwater. These results are in qualitative agreement with field observations by Uchiyama *et al.* [2000] who report the occurrence of high NO_3^- concentrations near the shore of Hasaki Beach in Japan, which they attribute to nitrification in the inland aerobic aquifer. Toward the shoreline, dissolved N in the freshwater part mixes with N supplied from the mineralization of organic matter from the sea bottom, analogous to our modeled NH_4^+ -rich seawater end-member. A net removal of modeled PO_4 is observed along the oxic/anoxic interface (Figure 4h) since PO_4 is adsorbed on the iron oxides that form at the redox boundary (not shown). This retention of PO_4 gives rise to a restricted landward penetration of the seawater PO_4 front (Figure 3f).

[16] The nutrient distributions and species profiles obtained in case 3, where anoxic groundwater meets oxic seawater, are given in Figures 3g–3i and 4k–4o. Here significant NO_3^- attenuation through denitrification is observed in the anoxic aquifer (Figure 3g). Comparison of the NO_3^- and NH_4^+ profiles with the “conservative” profiles indicates the occurrence of both nitrification and denitrification along the redox front. At the seaward boundary, denitrification lowers the peak NO_3^- concentration from ~ 0.06 mM to ~ 0.02 mM at a depth of 1 m while a new NO_3^- peak develops at a depth of ~ 3 m because of nitrification (Figure 4k). The upward shift in the NH_4^+ plume also reflects the occurrence of nitrification and denitrification, with a depletion of NH_4^+ at a depth of ~ 3 m and a production at ~ 1 m (Figure 4l and Table 2). The PO_4 plume is attenuated through sorption to concentrations as low as

0.005 mM prior to coastal discharge. Significant removal of PO_4 through adsorption is also often observed in field studies. For example, the maximum P concentration in SGD in the Perth area, Australia, was less than $2 \mu\text{g L}^{-1}$ ($\sim 0.065 \mu\text{M}$), since most of the groundwater P was precipitated or adsorbed in regions with Fe-rich sediments [Johannes, 1980]. Similarly, in the subterranean estuary of Waquoit Bay, Massachusetts, the formation of an “Iron Curtain” scavenges the groundwater PO_4 prior to its discharge into the coastal zone [Charette and Sholkovitz, 2002; Spiteri *et al.*, 2006]. As a result of nitrification, denitrification and PO_4 adsorption, the depths of the NO_3^- and NH_4^+ - PO_4 peaks at the seaward boundary are reversed relative to their original position at the landward source side. Thus a more reducing NH_4^+ - PO_4 plume overlies a more oxidizing NO_3^- plume as observed in the subterranean estuary of Waquoit Bay [Spiteri *et al.*, 2007b].

[17] In a completely anoxic subterranean estuary (case 4; Figures 3j–3l and 4p–4t), most of the anthropogenic NO_3^- is removed, causing the plume maximum to drop from ~ 0.06 mM to 0.01 mM in the anoxic groundwater. Yet the shape of the profile is distinct from case 3, since there is no additional NO_3^- production from nitrification. Our model indicates an increase in the NH_4^+ peak due to DOM degradation, but virtually no PO_4 removal because of the absence of $\text{Fe}(\text{OH})_3$. The formation of $\text{Fe}(\text{OH})_3$ through alternative processes, such as Fe^{2+} denitrification, is investigated in section 3.2.2.

3.1.3. Nutrient Fluxes

[18] For each of the four cases outlined above, we compute the nutrient fluxes leaving the model domain across the seaward boundary as SGD (Figure 5a). Denitrification causes a fourfold drop in the NO_3^- fluxes from $\sim 4000 \mu\text{mol m}^{-2} \text{d}^{-1}$ in the predominantly oxic systems (cases 1 and 2), to $\sim 1000 \mu\text{mol m}^{-2} \text{d}^{-1}$ in anoxic groundwaters (cases 3 and 4). Nevertheless, owing to the relatively high NH_4^+ fluxes in cases 3 and 4, the total inorganic N flux in the latter two cases is still higher than in cases 1 and 2, reaching up to $5000 \mu\text{mol m}^{-2} \text{d}^{-1}$ (Figure 5a). This is on the same order of magnitude as the N fluxes reported by Krest *et al.* [2000] ($2400 \mu\text{mol m}^{-2} \text{d}^{-1}$) for a predominantly anoxic system in South Carolina. The N fluxes obtained in cases 1 to 4 fall within the range of 430 to $19000 \mu\text{mol m}^{-2} \text{d}^{-1}$ given by Valiela *et al.* [1992] and Charette *et al.* [2001]. The magnitude of the P efflux to coastal waters is strongly dependent on the redox conditions in the subterranean estuary (Figure 5a). In the completely anoxic case (case 4; $\sim 4000 \mu\text{mol m}^{-2} \text{d}^{-1}$), the efflux of P is more than 130 times larger than in oxic conditions (case 1; $\sim 30 \mu\text{mol m}^{-2} \text{d}^{-1}$). The latter is of similar magnitude to the P flux reported by Garrison *et al.* [2003] ($37 \mu\text{mol m}^{-2} \text{d}^{-1}$) for inner Kahana Bay, Hawaii, for which the redox conditions are, however, not specified.

[19] The freshwater component of SGD containing terrestrially derived nutrients is of most environmental and ecological concern, as it carries “new” nutrients to the coastal ocean. This freshwater mixes with the recirculated

Figure 3. Simulated 2-D distributions for NO_3^- , NH_4^+ , and PO_4 obtained for (a–c) case 1 (oxic groundwater–oxic seawater), (d–f) case 2 (oxic groundwater–anoxic seawater), (g–i) case 3 (anoxic groundwater–oxic seawater), and (j–l) case 4 (anoxic groundwater–anoxic seawater) at steady state with respect to the solute species. Note that the arrow in Figure 3f indicates the landward penetration of the seawater PO_4 if conservative conditions are assumed.

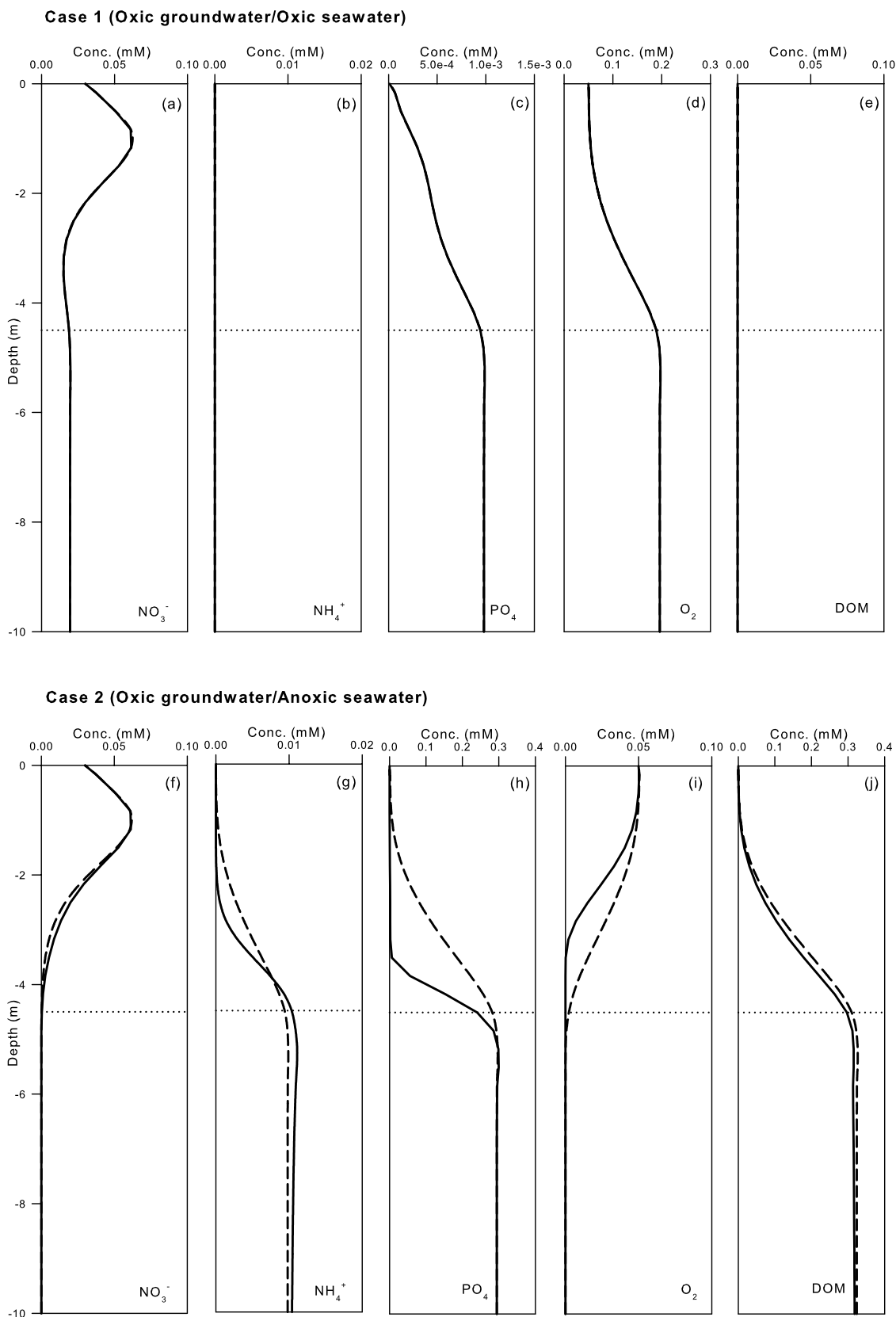


Figure 4. NO_3^- , NH_4^+ , PO_4 , O_2 , and DOM steady state concentration profiles at the seaward boundary for the top 10 m depth (solid lines) after a simulation period of 1000 d, compared with their respective conservative profiles (dashed lines). The horizontal dotted line indicates the (freshwater and recirculated seawater)-seawater interface, based on the x velocity profile in Figure 2c.

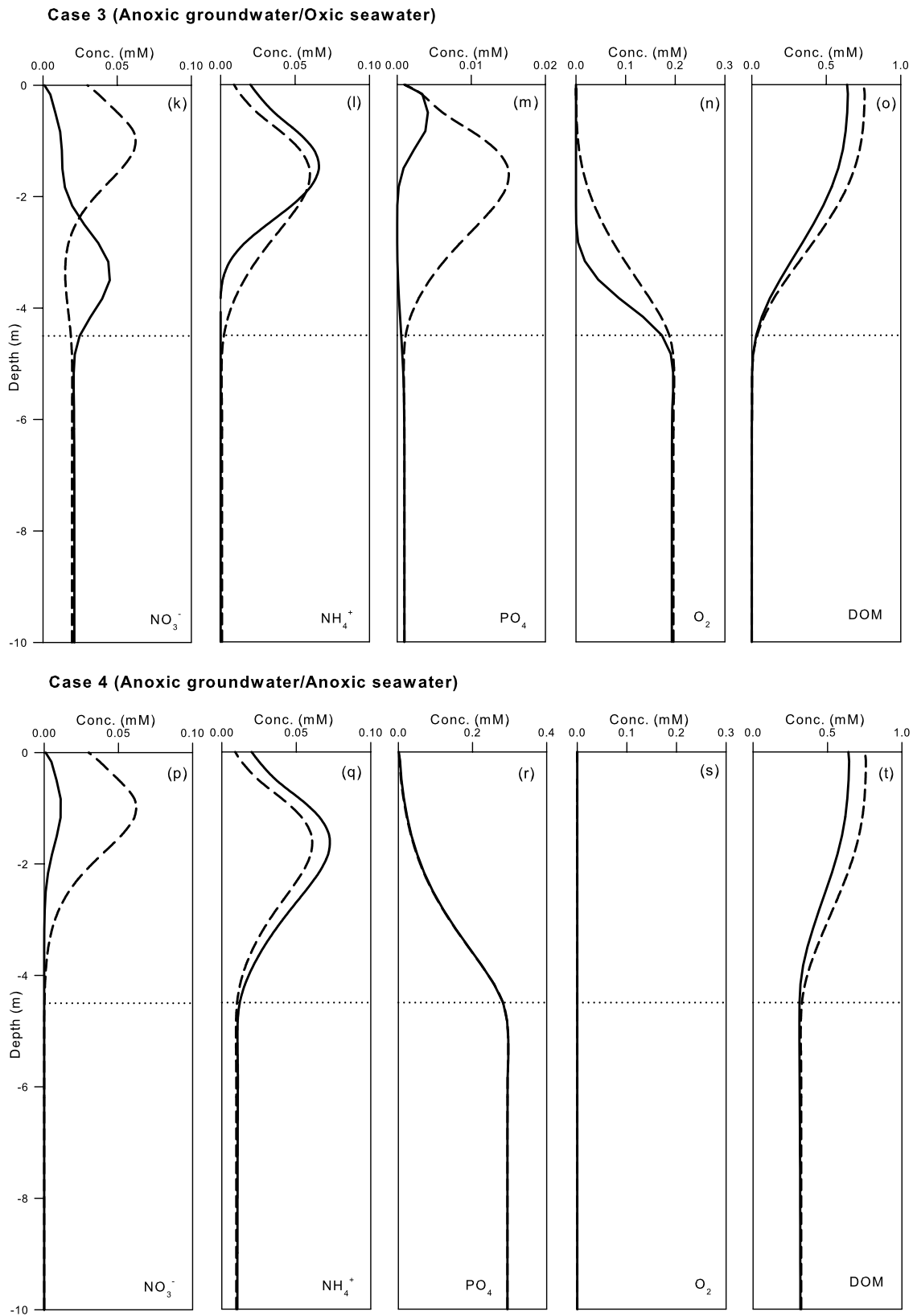


Figure 4. (continued)

seawater along the freshwater-seawater interface prior to discharge, hampering the distinction between “new” and recycled nutrient inputs. In cases with little nutrient transformation and significantly higher concentrations in the

freshwater end-member than in the sea, the magnitude of the landward/freshwater-supported fluxes and SGD are comparable (e.g., NO_3^- in cases 1 and 2; Figure 5b). Where subsurface nutrient transformation is important, N removal/

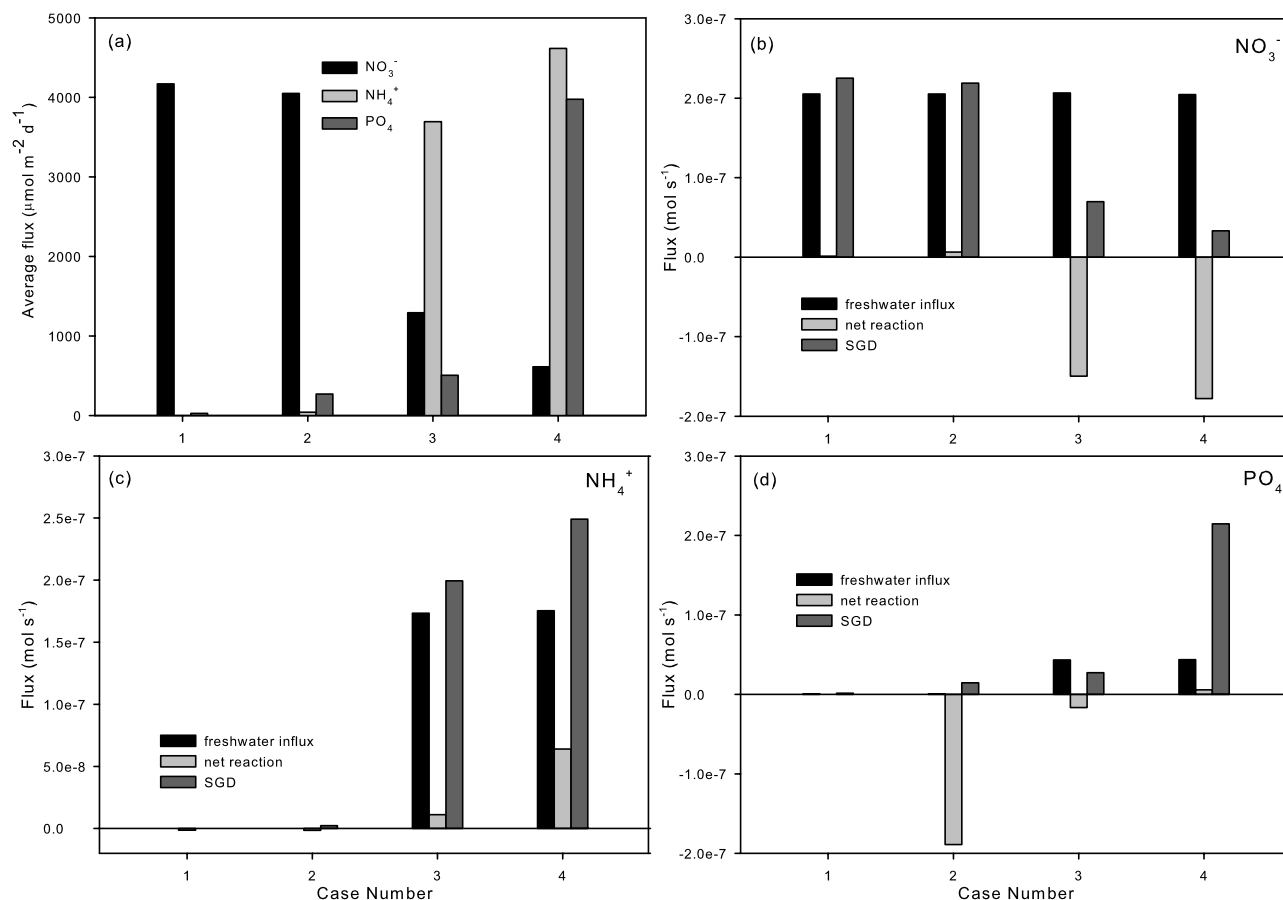


Figure 5. (a) Computed average advective nutrient fluxes leaving the seaward boundary as SGD in cases 1–4. The fluxes are expressed in $\mu\text{mol m}^{-2} \text{d}^{-1}$ for direct comparison with the coastal nutrient fluxes given by *Slomp and Van Cappellen* [2004]. Calculated influx rates at the freshwater boundary, net transformation rates due to reaction and efflux rates through SGD for (b) NO_3^- , (c) NH_4^+ , and (d) PO_4 in mol s^{-1} . Note that the NO_3^- increase between the freshwater influx and SGD in case 1 (Figure 5b) is supplied by the NO_3^- in seawater.

production roughly corresponds to the difference between SGD and the freshwater influx (e.g., NO_3^- in case 3 and NH_4^+ in case 4; Figure 5b and 5c, respectively), whereas the remainder is accounted for by the seawater influx. Recirculated seawater can also be a main contributor to nutrient loads, as is the case of P in cases 2 and 4 which are characterized by anoxic seawater (Figure 5d). Adsorption of P along the redox interface in cases 2 and 3 lowers the P flux through SGD by 1 order of magnitude when compared to the anoxic case 4.

3.1.4. N:P Ratios of SGD

[20] In agreement with a compilation of N:P ratios in coastal groundwater from the literature [*Slomp and Van Cappellen*, 2004], model results indicate highly variable N:P ratios of SGD (Figure 6) and highlight the importance of redox-dependent mitigation processes in coastal aquifers. In most contaminated sites, N:P ratios exceed the Redfield ratio, as illustrated in cases 1–3. In case 3, the N:P ratio increases drastically primarily because of localized retention of PO_4 on $\text{Fe}(\text{OH})_3$ at the interface. The N:P ratios lower than 16 obtained in anoxic conditions (case 4) are the result of extensive denitrification combined with the lack of PO_4 retention, and are consistent with observations in field studies by *Bugna et al.* [1996] and *Krest et al.* [2000].

3.1.5. Mixing Curves

[21] We extend the analysis of the modeled NO_3^- results for case 1 (section 3.1.2) through the application of mixing curves. By analogy to mixing models applied to surface estuaries [*Officer and Lynch*, 1981; *Shiller*, 1996; *Swarzenski et al.*, 2006], mixing curves (plots of concentrations against salinity/chlorinity) are often used in studies of elemental cycling in subterranean estuaries [*Capone and Bautista*, 1985; *Johannes and Hearn*, 1985; *Slater and Capone*, 1987; *Giblin and Gaines*, 1990; *Ullman et al.*, 2003; *Suzumura et al.*, 2000; *ArandaCirerol et al.*, 2006; *Charette and Sholkovitz*, 2006] to analyze chemical behavior along salinity gradients and to assess the contribution of dilution/mixing and biogeochemical processes. For instance, a linearly decreasing relationship between salinity and NO_3^- concentration is typically interpreted as the conservative dilution of high- NO_3^- groundwater with low NO_3^- seawater [*Johannes and Hearn*, 1985; *Giblin and Gaines*, 1990]. Concave nutrient concentrations profiles that fall below the conservative mixing line are assumed to indicate the occurrence of removal processes, such as denitrification [*Slater and Capone*, 1987; *Talbot et al.*, 2003] or PO_4 retention [*Suzumura et al.*, 2000].

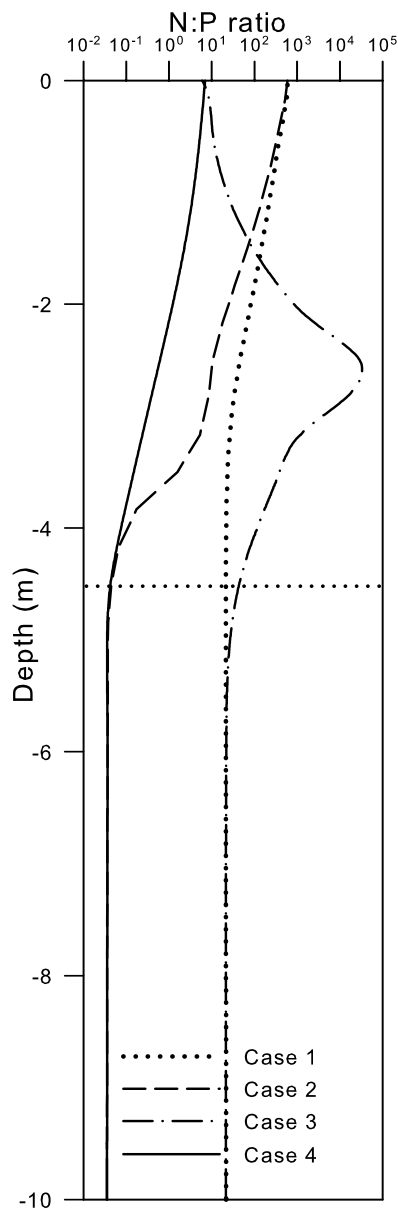


Figure 6. Simulated N:P profiles for cases 1–4 over the top 10 m. Note that the x axis is on a logarithmic scale. The horizontal dotted line indicates the (freshwater and recirculated seawater)-seawater interface, based on the x velocity profile in Figure 2c.

[22] The mixing curve obtained in the “conservative” simulation of case 1, in which NO_3^- is introduced as a point source (Figure 7b) is compared to a similar “conservative” simulation, in which the freshwater NO_3^- source is evenly distributed along the landward boundary (Figure 7a), representing a diffuse source analogous to agricultural activities. As expected, a linearly decreasing relationship between NO_3^- and salinity is obtained in the latter scenario (Figure 7c), implying the conservative mixing of freshwater and seawater NO_3^- end-members. However, even though transport is essentially conservative and all reactions are “switched off” in both simulations, the data points for the scenario with a point source fall below the mixing line (Figure 7d). This might be misinterpreted as resulting from the biogeo-

chemical removal of NO_3^- , such as through denitrification. Limited mixing of the point source NO_3^- plume alone leads to low-salinity high- NO_3^- conditions in the freshwater plume, a low-salinity low- NO_3^- region in the groundwater outside the NO_3^- plume, and high-salinity low- NO_3^- waters in the seawater end-member. Thus, if the application of mixing curves to subsurface data does not fulfill the requirements established for surface estuaries, namely steady state, one dimensional and tidally averaged flux conditions [Officer, 1979], the interpretation of a deviation from a linear conservative relationship as an indicator of production or removal is incorrect.

3.2. Sensitivity Analyses

[23] Sensitivity analyses were performed to investigate the impact of a number of aquifer and reaction parameters on nutrient mitigation at the subsurface land-ocean interface. We specifically focus on the role of transverse dispersion, NO_3^- removal through alternative denitrification pathways, the effect of flow rate and DOM reactivity, as well as the role of precipitation as an additional removal pathway for P. An overview of all sensitivity analysis runs is given in Table 4.

3.2.1. Role of α_T

[24] Transverse dispersion reflects the degree of the interconnectedness, shape and size of the pore-scale network in a porous medium. Therefore it plays an important role in the dilution and mixing of the plumes emanating from point sources at the landward model boundary and in the extent of mixing between the freshwater and seawater along the interface. Despite its importance, it is usually poorly constrained, since it is difficult to measure [Benekos et al., 2006]. The effect of doubling α_T on the dilution and/or reaction involving nutrients is assessed in cases 2 and 3, which are both characterized by a redox interface. As expected, broadening of the freshwater-seawater interface, increased overlap between the groundwater and seawater species and more diffuse solute plumes are obtained (not shown). As a result of enhanced $\text{Fe}(\text{OH})_3$ precipitation along the broader redox interface, the amount of adsorbed P increases by 17% and 15% in cases 2 and 3, respectively, when compared to the baseline simulations. Similarly, enhanced mixing leads to higher nitrification and denitrification rates in case 3. The rates of nitrification and denitrification integrated over the whole domain increase by 30% and 24%, respectively, implying that changing α_T has a major impact also on the extent of geochemical transformation.

3.2.2. Alternative Denitrification Pathways

[25] Alternative pathways of NO_3^- removal involve its reaction with electron donors other than DOM, such as dissolved Fe^{2+} , H_2S , CH_4 or solid pyrite, FeS_2 [Appelo and Postma, 2005]. Although evidence of NO_3^- reduction by Fe^{2+} has been presented both in the field [Höhn et al., 2006] and experimentally [Vanek 1990; Straub et al., 1996], the exact reaction mechanism is still not fully understood [Korom, 1992; Postma, 1990]. However, model simulations including Fe^{2+} denitrification (Table 2) give rise to little additional NO_3^- removal in the setup presented by case 2 (Figure 8a). In contrast, the removal of PO_4 is enhanced substantially through sorption on the additional $\text{Fe}(\text{OH})_3$ produced through the oxidation of Fe^{2+} along the redox interface (Figures 8b and 8c).

[26] The effect of the sequential oxidation of pyrite with O_2 and NO_3^- as electron acceptors [Wriedt and Rode, 2006]

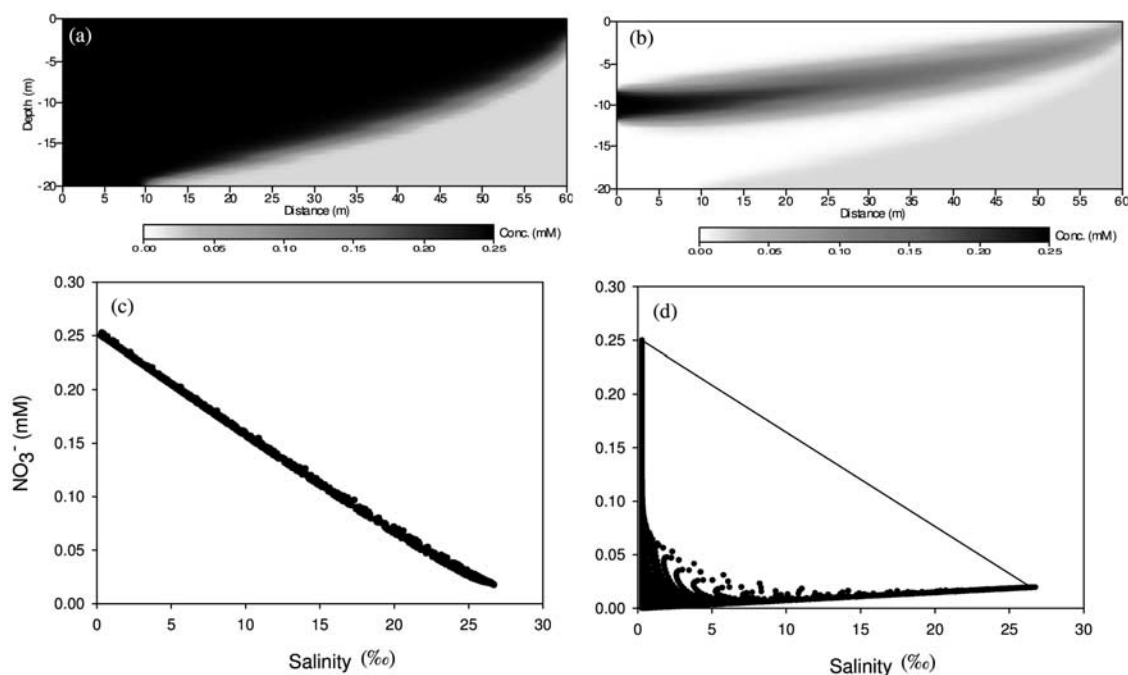


Figure 7. Simulated 2-D distribution for NO_3^- assuming a (a) diffuse and (b) point source along the freshwater boundary in case 1 and (c and d) their respective mixing curves (NO_3^- against salinity). The diagonal line in (Figure 6d) indicates the conservative mixing line.

(Table 2) on the extent of additional NO_3^- removal in case 3 is also investigated. To assess the potential role of the poorly constrained autotrophic pyrite denitrification in coastal aquifers, a uniform initial concentration of $10 \text{ mmol pyrite kg}^{-1}_{\text{solid}}$ [Appelo and Postma, 2005] is assumed throughout the whole coastal aquifer depicted by case 3. In this setting, pyrite denitrification enhances the removal of NO_3^- from the groundwater plume, and exceeds denitrification with DOM, in line with the field observations by Postma *et al.* [1991]. Similar to Fe^{2+} denitrification, pyrite oxidation strongly couples NO_3^- with PO_4 biogeochemistry through the formation of Fe^{2+} (Table 2), which precipitates as $\text{Fe}(\text{OH})_3$ at the oxic seawater boundary. Pyrite oxidation consumes O_2 , causing the seawater wedge to become anoxic and preventing the precipitation of $\text{Fe}(\text{OH})_3$ further inland along the freshwater-seawater redox boundary. Consequently, no net PO_4 removal from the freshwater plume through sorption occurs, whereas significant PO_4 removal is obtained at the seawater boundary of the model domain.

3.2.3. Damköhler Numbers: Effect of Flow Rate and DOM Reactivity

[27] To assess the interplay between transport and reaction on N dynamics in subterranean estuaries, or more specifically, the influence of groundwater flow rates and DOM reactivity on NO_3^- production/removal, two sets of sensitivity analyses are performed on case 3 where both nitrification and denitrification are active near the redox boundary. First, the value of k_{fox} is varied between $3 \times 10^{-10} \text{ s}^{-1}$ and $3 \times 10^{-8} \text{ s}^{-1}$, representing refractory and labile DOM, respectively. The flow conditions are identical to the baseline simulations, with a freshwater head at the landward model boundary of 0.4 m. Secondly, k_{fox} is kept constant at the baseline value of $3 \times 10^{-9} \text{ s}^{-1}$, but the freshwater head is varied from 0.24 to 1.5 m, resulting in a range of groundwater advective velocities from $0.1 \times 10^{-6} \text{ m s}^{-1}$ to $1.5 \times 10^{-6} \text{ m s}^{-1}$ at the left-hand-side boundary (Table 5). Here the same model domain as in the baseline simulations is used in all runs, except in run

Table 4. List of Sensitivity Analysis Runs

Run	Case	Parameter Changed/Reaction Added	Aim
1	2, 3	$\alpha_T = 0.1 \text{ m}$	to assess the effect of α_T on the extent of freshwater-seawater mixing and geochemical transformation
2	2	denitrification via Fe^{2+}	to assess the additional NO_3^- removal potential using Fe^{2+} as the electron donor
3	3	sequential pyrite oxidation and denitrification	to assess the roles of autotrophic (DOM) and heterotrophic (pyrite) denitrification
NG ^a	3	k_{fox} varied from $3.0 \times 10^{-8} \text{ s}^{-1}$ – $3.0 \times 10^{-10} \text{ s}^{-1}$	to assess the effect of DOM reactivity on NO_3^- removal
NG ^a	3	freshwater head varied from 0.24 to 1.5 m	to assess the effect of flow rate on denitrification
4	3, 4	hydroxyapatite precipitation	to assess the additional PO_4 removal potential through precipitation of P as $\text{Ca}(\text{PO}_4)_3\text{OH}$

^aNG, not given; see Table 5.

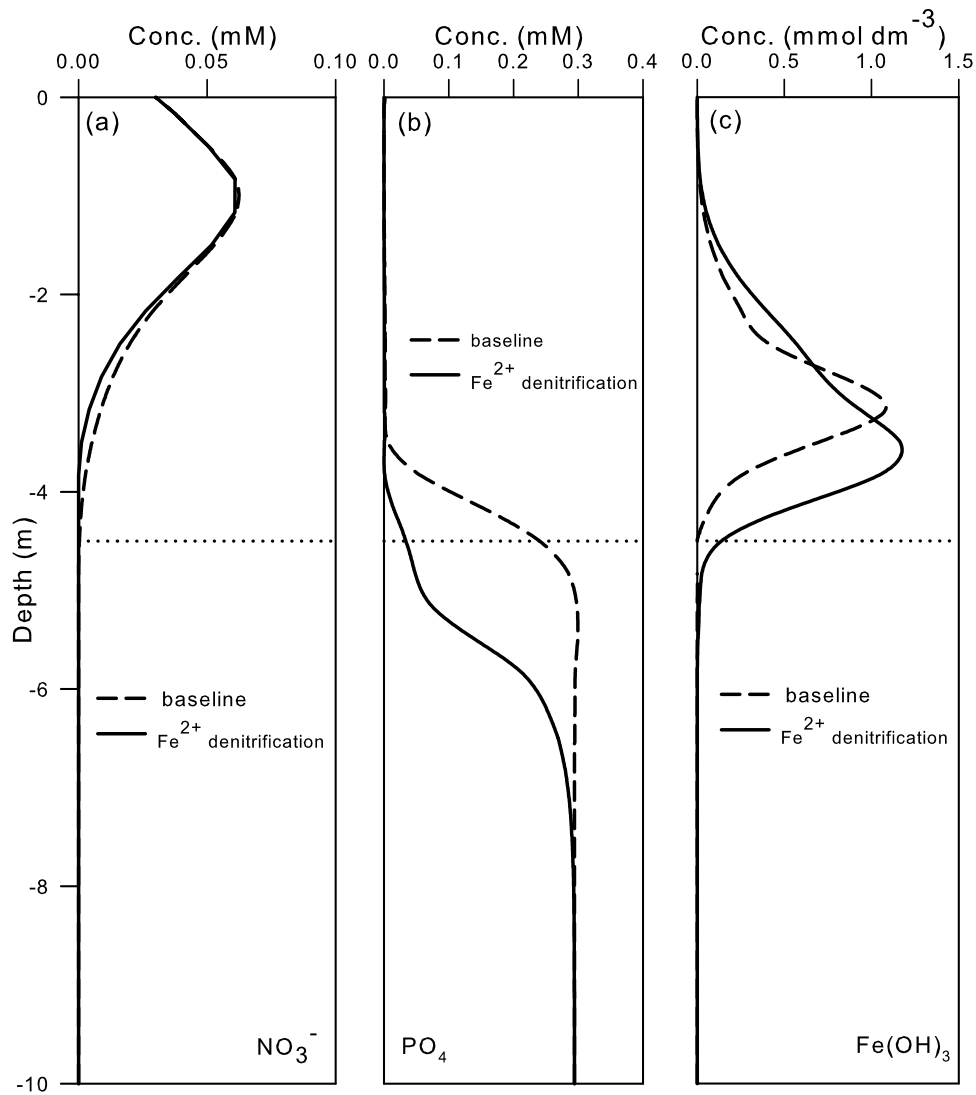


Figure 8. Profiles of (a) NO_3^- , (b) PO_4 , and (c) $\text{Fe}(\text{OH})_3$ over the top 10 m, obtained when Fe^{2+} denitrification is included in the reaction network (solid lines), compared to the baseline profiles (dashed lines) (case 2). The horizontal dotted line indicates the (freshwater and recirculated seawater)-seawater interface, based on the x velocity profile in Figure 2c.

numbers 1–3 (Table 5), where the model domain is extended to 100 m so that the steady state saltwater wedge does not interfere with the freshwater boundary.

[28] The rates of transport and reactions in the above simulations are compared by using the ratio of DOM degradation rate to groundwater flow rate, expressed as a dimensionless Damköhler number (Da) [Domenico and Schwartz, 1998; Ocampo *et al.*, 2006]:

$$Da = \frac{k_{\text{fox}} \cdot L}{v} \quad (1)$$

where in this particular case, k_{fox} (s^{-1}) is the rate constant for DOM decomposition, used as a proxy for denitrification rate, L (m) refers to the length of the flow path taken by the NO_3^- plume and v (m s^{-1}) is the advective groundwater velocity at the left-hand-side boundary. Damköhler numbers >1 correspond to reaction-controlled systems, whereas Da numbers <1 imply that the system is transport dominated. The Da numbers for the simulations in set 1 range from as

low as 0.08 to ~ 8.5 . In set 2, the maximum calculated Da is 2.35 (Table 5), since given our choice of model aquifer parameters, higher Da numbers can only be obtained if unrealistically low groundwater velocities are assumed.

[29] Figure 9a shows the total rate of NO_3^- production/removal through nitrification/denitrification (mol s^{-1}) at steady state, normalized to the freshwater NO_3^- influx (mol s^{-1}), as a function of Da for the first set of simulations (Table 5). The vertical dotted line at $Da = 1$ divides the domain into the transport-dominated zone to the left and the reaction-dominated zone to the right. At very small values of Da (Figure 9a), the ratio of NO_3^- removal to NO_3^- influx is ~ 0.1 , and NO_3^- travels almost conservatively. Here denitrification is inhibited by the low reactivity of DOM. Organic carbon limitation to denitrification is commonly reported in shallow groundwater aquifers and sandy near-shore sediments [e.g., Starr and Gillham, 1993; Slater and Capone, 1987; DeSimone and Howes, 1996; Portnoy *et al.*, 1998]. As the Da increases (Figure 9a), the extent of removal also increases, reaching near-complete removal at

Table 5. Parameters for “*Da* Simulations”: Case 3

Run	$k_{\text{fox}}, \text{s}^{-1}$	Freshwater Head, m	Groundwater Velocity, m s^{-1a}	<i>Da</i> (dimensionless) ^b
<i>Set 1</i>				
1	3.0×10^{-10}	0.4	2.2×10^{-7}	0.08
2	6.0×10^{-10}	0.4	2.2×10^{-7}	0.17
3	1.0×10^{-9}	0.4	2.2×10^{-7}	0.30
4	1.5×10^{-9}	0.4	2.2×10^{-7}	0.42
5	3.0×10^{-9}	0.4	2.2×10^{-7}	0.85
6	9.0×10^{-9}	0.4	2.2×10^{-7}	2.54
7	1.5×10^{-8}	0.4	2.2×10^{-7}	4.23
8	3.0×10^{-8}	0.4	2.2×10^{-7}	8.45
<i>Set 2</i>				
1	3.0×10^{-9}	0.24 (0.4) ^c	1.3×10^{-7}	2.35
2	3.0×10^{-9}	0.27 (0.45) ^c	1.7×10^{-7}	1.86
3	3.0×10^{-9}	0.3 (0.5) ^c	2.0×10^{-7}	1.54
4	3.0×10^{-9}	0.4	2.2×10^{-7}	0.83
5	3.0×10^{-9}	0.5	3.4×10^{-7}	0.55
6	3.0×10^{-9}	0.6	4.6×10^{-7}	0.41
7	3.0×10^{-9}	0.8	6.9×10^{-7}	0.27
8	3.0×10^{-9}	1.0	9.2×10^{-7}	0.20
9	3.0×10^{-9}	1.2	1.2×10^{-6}	0.16
10	3.0×10^{-9}	1.5	1.5×10^{-6}	0.12

^aRefers to the advective groundwater velocity at the landward boundary.

^bBecause of the tangential path taken by the groundwater NO_3^- plume as it bends upward over the seawater wedge, *L* in equation (1) is set typically at 62 m. *L* = 105 m.

^cDomain length extended from 60 to 100 m. The values in parentheses refer to the freshwater head imposed over 100 m.

Da ~8, driven by higher DOM reactivity. Nitrification, which supplies an additional source of NO_3^- as also observed in the field by *Nowicki et al.* [1999], increases steadily as an indirect result of the enhanced reactivity of DOM (Figure 9a, top curve).

[30] The results from the second set of simulations (Table 5 and Figure 9b) show a similar trend in the relative NO_3^- production/removal on either side of the vertical line at *Da* = 1. Because of the high groundwater flow velocities, the rate of freshwater NO_3^- influx across the landward boundary at low *Da* numbers is higher than the rate of NO_3^- removal through denitrification. This is in line with field studies by *Giblin and Gaines* [1990], who observed that at high groundwater flow rates, denitrification in sandy sediments was unable to reduce significantly the external septic system-derived N loading, leading to the conservative discharge of NO_3^- . The extent of the NO_3^- production and removal relative to the freshwater influx of NO_3^- increases with decreasing groundwater velocities (Figure 9b). This gives rise to the near-complete removal of the NO_3^- plume at low groundwater velocities, including the additional NO_3^- supplied by nitrification.

3.2.4. Phosphorus Removal Through Hydroxyapatite Precipitation

[31] Generally, discharge of P is limited because of adsorption on Fe oxides. However, in some cases, especially in carbonate aquifers [e.g., *Lapointe et al.*, 1990; *Cable et al.*, 2002], additional PO_4 removal due to precipitation of minerals (such as, hydroxyapatite and carbonate fluorapatite) may play a role. We illustrate the importance of precipitation of hydroxyapatite as an additional removal process, using the setup defined in cases 3 and 4. In both scenarios, hydroxyapatite precipitates in the saltwater wedge when a pH of 8.2 is assumed for seawater [*Millero and Sohn*, 1992] with salinity >25‰, and pH 7.0 for fresh and brackish water. However, the

amount of precipitated solid differs in the two cases (Figure 10a), mainly because of the Ca^{2+} and PO_4 concentrations assumed for the different redox conditions (Table 1). The modeled precipitation of hydroxyapatite in seawater may be slightly overestimated since at pH 8.2, ~80% of PO_4 is in the form of HPO_4^{2-} [*Kester and Pytkowicz*, 1967] (Table 2). Although HPO_4^{2-} accounts for ~50% of PO_4 in the freshwater end-member, hydroxyapatite precipitation is limited by the low freshwater Ca^{2+} concentration. The most effective removal occurs in the completely anoxic case, where the accumulation of hydroxyapatite at a depth of 10 m after 1000 d is ~3.0 mmol dm^{-3} (1.13 $\mu\text{mol g}^{-1}$). Extensive P attenuation through the formation of cryptocrystalline calcium phosphate is also observed in an anoxic, saline Floridian aquifer, where almost complete removal of dissolved wastewater phosphorus occurs [*Cable et al.*, 2002]. The concentration of PO_4 in the groundwater plume assumed in case 3 (Table 1) is not high enough to trigger much hydroxyapatite precipitation upon interaction with the elevated seawater Ca^{2+}

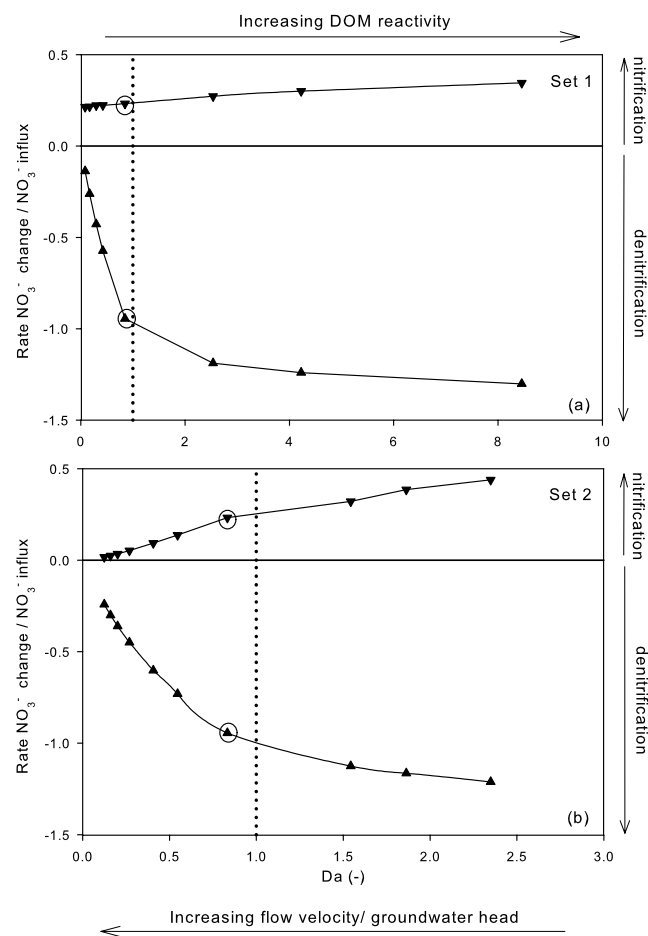


Figure 9. Ratio of rate of NO_3^- production/removal to freshwater NO_3^- influx rate in $\text{mol s}^{-1}/\text{mol s}^{-1}$ as a function of the *Da*. Nitrification is denoted by downward pointing triangles; denitrification is denoted by upward pointing triangles. (a) Results obtained by varying DOM reactivity. (b) Freshwater head varied (Table 5, case 3). Note that the encircled points in Figure 9a are identical to those in Figure 9b. The vertical line at *Da* = 1 separates the transport- and reaction-dominated domains.

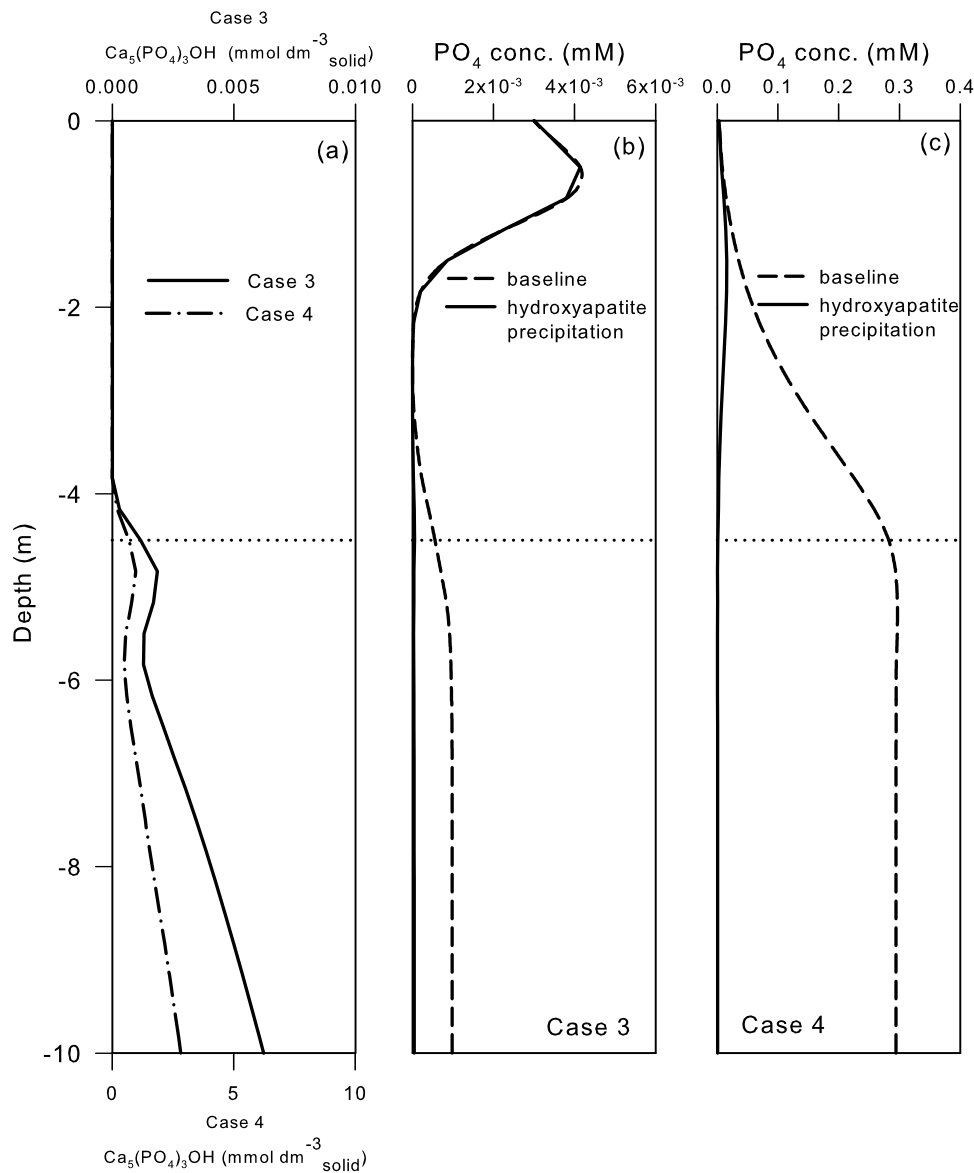


Figure 10. Simulated concentration profiles of (a) precipitated hydroxyapatite obtained for sensitivity analysis run number 4 in Table 4 (cases 3 and 4). Note the two separate x axis scales for case 3 (top) and case 4 (bottom). (b and c) Extent of PO_4 removal along the seawater boundary in cases 3 and 4, respectively, as a result of hydroxyapatite precipitation (solid line), when compared to the baseline simulations (dashed line). The horizontal dotted line indicates the (freshwater and recirculated seawater)-seawater interface, based on the x velocity profile in Figure 2c.

concentrations along the redox interface. This implies that PO_4 adsorption on Fe oxides is still the major P removal pathway in the groundwater part of a subterranean estuary characterized by anoxic groundwater and oxic seawater.

4. Conclusions

[32] This study illustrates that biogeochemical processes in subterranean estuaries can have a significant influence on the discharge of nutrients into coastal waters. Despite the simplified representation of the field conditions, modeled nutrient dynamics are rather complex. The results obtained with a 2-D density-dependent reactive transport model show that the fate of N and P in the four idealized subterranean estuaries strongly depends on the redox conditions along the freshwa-

ter-seawater continuum. However, the extent of freshwater and seawater mixing, assessed by studying the response of nutrient discharge under different transverse dispersivities and flow rates, also plays a role in determining nutrient transformation and removal. We also show that the application of mixing curves to evaluate nutrient production or removal in subterranean estuaries should be avoided, since a deviation from the conservative mixing line could be merely the result of the nature of the nutrient source, practical restrictions on sample collection and consequent limited knowledge on the solute concentration fields.

[33] Denitrification and P sorption are two key processes that determine the extent of nutrient removal. Denitrification is coupled not only to the reactivity of DOM, but also to the flow dynamics, since the efficiency of NO_3^- removal

increases drastically at lower groundwater flow rates. Moreover, denitrification with Fe^{2+} and FeS_2 as electron donors couples the N and P biogeochemistry through the precipitation of $\text{Fe}(\text{OH})_3$ as a by-product. P sorption is mainly important in settings where a redox interface is formed when groundwater and seawater with different redox conditions interact, whereas P mineral precipitation in the form of hydroxyapatite predominates in the seawater part. The overall effect of the various redox processes occurring within each subterranean estuary is reflected in the molar N:P ratio of the SGD, spanning from ~ 0.03 to 30000. The results highlight the need to account for redox-dependent transformation and removal processes for N and P when estimating rates of SGD of nutrients based on groundwater velocities and nutrient concentrations in field studies.

Appendix A: Mathematical Equations Used in Finite Element Reactive Transport Model

[34] The equation of continuity for fluid flow in a saturated porous medium is given by

$$-\left[\frac{\partial(\rho q_x)}{\partial x} + \frac{\partial(\rho q_y)}{\partial y} + \frac{\partial(\rho q_z)}{\partial z}\right] = \frac{\partial(\phi\rho)}{\partial t} \quad (\text{A1})$$

where t is time (T) and ϕ is the effective porosity of the medium (–). Using Darcy's Law, the flow equation for three-dimensional laminar flow is described as [e.g., Bear, 1972]

$$q = -\frac{\kappa}{\mu}(\nabla P - \rho g) \quad (\text{A2})$$

where q is the Darcy flux (LT^{-1}), κ is the second rank intrinsic permeability tensor (L^2), μ is the dynamic viscosity of water ($\text{M L}^{-1} \text{T}^{-1}$), P is pressure ($\text{M L}^{-1} \text{T}^{-2}$), g is the gravitational acceleration (L T^{-2}) and ρ is density (M L^{-3}).

[35] In the finite element reactive transport model, the equation of state for seawater, which relates the density of the fluid (ρ in kg m^{-3}) to temperature (T in $^\circ\text{C}$) and salinity (S in psu), is given by an approximation to the UNESCO equation, at 1 bar pressure:

$$\rho(T, S) = 1000.0821 + 0.7925S - 0.0324(T - 4) - 0.0052(T - 4)^2 - 0.0021S(T - 4) \quad (\text{A3})$$

where the aquifer temperature is assumed constant at 10°C .

[36] Since the fluid density is a function of salinity, and solute concentrations may change in response to the groundwater flow field, the advection-dispersion equation is used to describe the salinity field:

$$\frac{\partial\phi C_i}{\partial t} = \nabla \cdot (D\phi\nabla C_i) - \nabla \cdot (\phi\nu C_i) \quad (\text{A4})$$

where C is the concentration of a solute (e.g., salinity), D is the dispersion tensor ($\text{L}^2 \text{T}^{-1}$) and ν is equal to $\frac{q}{\phi}$. D is defined as

$$D_{ij} = (\alpha_L - \alpha_T) \frac{v_i v_j}{|v|} + \alpha_T |v| \delta_{ij} \quad (\text{A5})$$

where δ_{ij} , α_L , α_T are Kronecker symbol, longitudinal and transverse dispersivities [L^2], respectively. For a reactive solute, the right-hand side of equation (A4) contains an additional rate term, R_i . The reaction rates are calculated explicitly, i.e., computed as described in Table 2 from the known concentration fields at the previous time step. Solid species are assumed immobile and are thus only produced/consumed locally.

[37] **Acknowledgments.** We would like to thank T. Torgersen, D. Kent, W. C. Burnett, and two anonymous reviewers for their valuable comments, which helped to improve the manuscript. C. M. acknowledges support by Georgia Sea Grant of the National Sea Grant College Program of the U.S. Department of Commerce's National Oceanic and Atmospheric Administration under NOAA grant NA04OAR4170033. The views herein do not necessarily reflect the views of any of those organizations. C. P. S. was supported by the Royal Netherlands Academy of Arts and Sciences and the Netherlands Organization for Scientific Research (VIDI-grant).

References

- Appelo, C. A. J., and D. Postma (2005), *Geochemistry, Groundwater and Pollution*, A. A. Balkema, Rotterdam, Netherlands.
- ArandaCirerol, N., J. A. Herrera-Silveira, and F. A. Comin (2006), Nutrient water quality in a tropical coastal zone with groundwater discharge, northwest Yucatán, Mexico, *Estuarine Coastal Shelf Sci.*, *68*, 445–454.
- Bear, J. (1972), *Dynamics of Fluids in Porous Media*, Elsevier, New York.
- Benekos, I. D., O. A. Cirpka, and P. K. Kitanidis (2006), Experimental determination of transverse dispersivity in a helix and a cochlea, *Water Resour. Res.*, *42*, W07406, doi:10.1029/2005WR004712.
- Berner, E. K., and R. A. Berner (1996), *Global Environment: Water, Air and Geochemical Cycles*, Prentice-Hall, Upper Saddle River, New Jersey.
- Boehm, A. B., A. Paytan, G. G. Shellenberger, and K. A. Davis (2006), Composition and flux of groundwater from a California beach aquifer: Implications for nutrient supply to the surf zone, *Cont. Shelf Res.*, *26*, 269–282.
- Bugna, G. C., J. P. Chanton, J. E. Cable, W. C. Burnett, and P. H. Cable (1996), The importance of groundwater discharge to the methane budgets of nearshore and continental shelf waters of the northeastern Gulf of Mexico, *Geochim. Cosmochim. Acta*, *23*, 4735–4746.
- Burnett, W. C., et al. (2006), Quantifying submarine groundwater discharge in the coastal zone via multiple methods, *Sci. Total Environ.*, *367*, 498–593.
- Burnett, W. C., G. Wattayakorn, M. Taniguchi, H. Dulaiova, P. Sojisuporn, S. Rungsupa, and T. Ishitobi (2007), Groundwater-derived nutrient inputs to the Upper Gulf of Thailand, *Cont. Shelf Res.*, *27*, 176–190.
- Cable, J. E., W. C. Burnett, J. P. Chanton, and G. L. Weatherly (1996), Estimating groundwater discharge into the northeastern Gulf of Mexico using radon-222, *Earth Planet. Sci. Lett.*, *144*, 591–604.
- Cable, J. E., D. R. Corbett, and M. M. Walsh (2002), Phosphate uptake in coastal aquifers: A fresh look at wastewater management, *Limnol. Oceanogr. Bull.*, *11*, 1–4.
- Capone, D. G., and M. F. Bautista (1985), A groundwater source of nitrate in nearshore marine sediments, *Nature*, *313*, 214–216.
- Capone, D. G., and J. M. Slater (1990), Interannual patterns of water table height and groundwater derived nitrate in nearshore sediments, *Biogeochemistry*, *10*, 277–288.
- Charette, M. A., and E. R. Sholkovitz (2002), Oxidative precipitation of groundwater-derived ferrous iron in the subterranean estuary of a coastal bay, *Geophys. Res. Lett.*, *29*(10), 1444, doi:10.1029/2001GL014512.
- Charette, M. A., and E. R. Sholkovitz (2006), Trace element cycling in a subterranean estuary: part 2. Geochemistry of the pore water, *Geochim. Cosmochim. Acta*, *70*, 811–826.
- Charette, M. A., K. O. Buesseler, and J. E. Andrews (2001), Utility of radium isotopes for evaluating the input and transport of groundwater-derived nitrogen to a Cape Cod estuary, *Limnol. Oceanogr.*, *46*, 465–470.
- Charette, M. A., E. R. Sholkovitz, and C. M. Hansel (2005), Trace element cycling in a subterranean estuary: part 1. Geochemistry of the permeable sediments, *Geochim. Cosmochim. Acta*, *69*, 2095–2109.
- Church, T. H. (1996), An underground route for the water cycle, *Nature*, *380*, 579–580.

- Corbett, D. R., J. P. Chanton, W. C. Burnett, K. S. Dillon, C. Rutkowski, and J. Fourqurean (1999), Patterns of groundwater discharge into Florida Bay, *Limnol. Oceanogr.*, *44*, 973–1185.
- Crusius, J., D. Koopmans, J. Bratton, M. A. Charette, K. Kroeger, P. Henderson, L. Ryckman, K. Halloran, and J. Coleman (2005), Submarine groundwater discharge to a small estuary estimated from radon and salinity measurements and a box model, *Biogeosciences*, *2*, 141–157.
- DeSimone, L. A., and B. L. Howes (1996), Denitrification and nitrogen transport in a coastal aquifer receiving wastewater discharge, *Environ. Sci. Technol.*, *30*, 1152–1162.
- Domenico, P., and F. W. Schwartz (1998), The equations of mass transport, in *Physical and Chemical Hydrogeology*, John Wiley, Hoboken, N. J.
- Frind, E. O., W. H. M. Duijnsveld, O. Strelbel, and J. Boettcher (1990), Modelling of multi-component transport with microbial transformation in groundwater: The Fuhrberg case, *Water Resour. Res.*, *26*, 1707–1719.
- Frossard, E., M. Brossard, M. J. Hedley, and A. Metherell (1995), Reactions controlling the cycling of P in soils, in *Phosphorus In The Global Environment*, edited by H. Tiessen, pp. 107–138, John Wiley, Hoboken, N. J.
- Garrison, G. H., C. R. Glenn, and G. M. McMurty (2003), Measurement of submarine groundwater discharge in Kahana Bay, O'ahu, Hawai'i, *Limnol. Oceanogr.*, *48*, 920–928.
- Giblin, A. E., and A. G. Gaines (1990), Nitrogen inputs to a marine embayment: The importance of groundwater, *Biogeochemistry*, *10*, 309–328.
- Höhn, R., M. Isenbeck-Schröter, D. B. Kent, J. A. Davis, R. Jakobsen, S. Jann, V. Niedan, C. Scholz, S. Stadler, and A. Tretner (2006), Tracer test with As(V) under variable redox conditions controlling arsenic transport in the presence of elevated ferrous iron concentrations, *J. Contam. Hydrol.*, *88*, 36–54.
- Howarth, R. W. (1988), Nutrient limitation of net primary production in marine ecosystems, *Annu. Rev. Ecol. Syst.*, *19*, 89–110.
- Inskip, W. P., and J. C. Silvertooth (1988), Kinetics of hydroxyapatite precipitation at pH 7.4 to 8.4, *Geochim. Cosmochim. Acta*, *52*, 1883–1893.
- Johannes, R. E. (1980), The ecological significance of the sub-marine discharge of groundwater, *Mar. Ecol. Prog. Ser.*, *3*, 365–373.
- Johannes, R. E., and C. J. Hearn (1985), The effect of submarine groundwater discharge on nutrient and salinity regimes in a coastal lagoon off Perth, Western Australia, *Estuarine Coastal Shelf Sci.*, *21*, 789–800.
- Kamei, G., and H. Ohmoto (2000), The kinetics of reactions between pyrite and O₂-bearing water revealed from in situ measurements of DO, Eh and pH in a closed system, *Geochim. Cosmochim. Acta*, *64*, 2585–2601.
- Kester, D. R., and R. M. Pytkowicz (1967), Determination of the apparent dissociation constants of phosphoric acid in seawater, *Limnol. Oceanogr.*, *12*, 243–252.
- Korom, S. F. (1992), Natural denitrification in the saturated zone: A review, *Water Resour. Res.*, *28*, 1657–1668.
- Krest, J. M., W. S. Moore, L. R. Gardner, and J. T. Morris (2000), Marsh nutrient export supported by groundwater discharge evidence from radium isotope measurements, *Global Biogeochem. Cycles*, *14*, 167–176.
- Krom, M. D., and R. A. Berner (1980), Adsorption of phosphate in anoxic marine sediments, *Limnol. Oceanogr.*, *25*, 797–806.
- Lapointe, B. E., J. D. O'Connell, and G. S. Garrett (1990), Nutrient couplings between on-site sewage disposal systems, groundwaters, and near-shore surface waters of the Florida Keys, *Biogeochemistry*, *10*, 289–307.
- LaRoche, J., R. Nuzzi, R. Waters, K. Wyman, P. G. Falkowski, and D. W. R. Wallace (1990), Brown tide blooms in Long Island's coastal waters linked to interannual variability in groundwater flow, *Global Change Biol.*, *3*, 397–410.
- Meile, C., and K. Tuncay (2006), Scale dependence of reaction rates in porous media, *Adv. Water Resour.*, *29*, 62–71.
- Millero, F. J., and M. L. Sohn (1992), *Chemical Oceanography*, CRC Press, Boca Raton, Fla.
- Moore, W. S. (1999), The subterranean estuary: A reaction zone of groundwater and sea water, *Mar. Chem.*, *65*, 111–125.
- Nowicki, B. L., E. Requitina, D. van Keuren, and J. Portnoy (1999), The role of sediment denitrification in reducing groundwater-derived nitrate inputs to Nauset Marsh Estuary, Cape Cod, Massachusetts, *Estuaries*, *22*, 245–259.
- Nyvang, V. (2003), Redox processes at the salt-/freshwater interface in an anaerobic aquifer, Ph.D. dissertation, Technical Univ. of Denmark, Lyngby.
- Oberdorfer, J. A., M. A. Valentino, and S. V. Smith (1990), Groundwater contribution to the nutrient budget of Tomales Bay, California, *Biogeochemistry*, *10*, 199–216.
- Ocampo, C. J., C. E. Oldham, and M. Sivapalan (2006), Nitrate attenuation in agricultural catchments: Shifting balances between transport and reaction, *Water Resour. Res.*, *42*, W01408, doi:10.1029/2004WR003773.
- Officer, C. B. (1979), Discussion of the behaviour of nonconservative dissolved constituents in estuaries, *Estuarine Coastal Mar. Sci.*, *9*, 91–94.
- Officer, C. B., and D. R. Lynch (1981), Dynamics of mixing in estuaries, *Estuarine Coastal Shelf Sci.*, *12*, 525–533.
- Paeli, H. (1997), Coastal eutrophication and harmful algal blooms: Importance of atmospheric deposition and groundwater as new nitrogen and other nutrient sources, *Limnol. Oceanogr.*, *42*, 1154–1165.
- Paytan, A., G. G. Shellenbarger, H. J. Street, M. E. Gonneea, K. Davis, B. M. Young, and W. S. Moore (2006), Submarine groundwater discharge an important source of new nutrients to coral reef ecosystems, *Limnol. Oceanogr.*, *51*, 343–348.
- Portnoy, J. W., B. L. Nowicki, C. T. Roman, and D. W. Urish (1998), The discharge of nitrate-contaminated groundwater from developed shoreline to marsh-fringed estuary, *Water Resour. Res.*, *34*, 3095–3104.
- Postma, D. (1990), Kinetics of nitrate by detrital Fe(II)-silicates, *Geochim. Cosmochim. Acta*, *54*, 903–908.
- Postma, D., C. Boesen, H. Kristiansen, and F. Larsen (1991), Nitrate reduction in an unconfined sandy aquifer: Water chemistry, reduction processes and geochemical modeling, *Water Resour. Res.*, *27*, 2027–2045.
- Reddy, J. N. (1993), *An Introduction to the Finite Element Method*, 2nd ed., McGraw-Hill, New York.
- Scheidegger, A. (1961), General theory of dispersion in porous media, *J. Geophys. Res.*, *66*, 3273–3278.
- Scientific Committee on Oceanic Research (2004), Submarine groundwater discharge: Management implications, measurements and effects, *IHP Ser. Groundwater 5*, United Nations Educ., Sci. and Cult. Organ., Paris.
- Sewell, P. L. (1982), Urban groundwater as a possible nutrient source for an estuarine benthic algal bloom, *Estuarine Coastal Shelf Sci.*, *15*, 569–576.
- Shiller, A. M. (1996), The effect of recycling traps and upwelling on estuarine chemical flux estimates, *Geochim. Cosmochim. Acta*, *60*, 3177–3185.
- Slater, J. M., and D. G. Capone (1987), Denitrification in aquifer soil and nearshore marine sediments influenced by groundwater nitrate, *Appl. Environ. Microbiol.*, *53*, 1292–1297.
- Slomp, C. P., and P. Van Cappellen (2004), Nutrient inputs to the coastal ocean through submarine groundwater discharge: Controls and potential impact, *J. Hydrol.*, *295*, 64–86.
- Spiteri, C., P. Regnier, C. P. Slomp, and M. A. Charette (2006), pH-dependent iron oxide precipitation in a subterranean estuary, *J. Geochem. Explor.*, *88*, 399–403.
- Spiteri, C., C. P. Slomp, P. Regnier, C. Meile, and P. Van Cappellen (2007a), Modelling the geochemical fate and transport of wastewater-derived phosphorus in contrasting groundwater systems, *J. Contam. Hydrol.*, *92*, 87–108.
- Spiteri, C., C. P. Slomp, M. A. Charette, K. Tuncay, and C. Meile (2007b), Reactive transport modeling of flow and nutrient dynamics in a coastal aquifer (Waquoit Bay, MA, USA), paper presented at International Conference on Water Pollution in Natural Porous Media at Different Scales: Assessment of Fate, Impact and Indicators, COST, Barcelona, April 2007.
- Starr, R. C., and R. W. Gillham (1993), Denitrification and organic carbon availability in two aquifers, *Ground Water*, *31*, 934–947.
- Straub, K. L., M. Benz, B. Schink, and F. Widdel (1996), Anaerobic, nitrate-dependent microbial oxidation of ferrous iron, *Appl. Environ. Microbiol.*, *62*, 1458–1460.
- Suzumura, M., S. Ueda, and E. Sumi (2000), Control of phosphate concentration through adsorption and desorption processes in groundwater and seawater mixing at sandy beaches in Tokyo Bay, Japan, *J. Oceanogr.*, *56*, 667–673.
- Swarczewski, P. W., W. H. Orem, B. F. McPherson, M. Baskaran, and Y. Wan (2006), Biogeochemical transport in the Loxahatchee River estuary, Florida: The role of submarine groundwater discharge, *Mar. Chem.*, *101*, 248–265.
- Talbot, J. M., K. D. Kroeger, A. Rago, M. C. Allen, and M. A. Charette (2003), Nitrogen flux and speciation through the subterranean estuary of Waquoit Bay, Massachusetts, *Biol. Bull.*, *205*, 244–245.
- Taniguchi, M., W. C. Burnett, J. E. Cable, and J. V. Turner (2002), Investigation of submarine groundwater discharge, *Hydrol. Processes*, *16*, 2115–2129.
- Uchiyama, Y., K. Nadaoka, P. Rolke, K. Adachi, and H. Yagi (2000), Submarine groundwater discharge into the sea and associated nutrient transport in a sandy beach, *Water Resour. Res.*, *36*, 1467–1479.
- Ueda, S., U. G. Chun-Sim, M. Suzumura, and E. Sumi (2003), Denitrification in a seashore sandy deposit influenced by groundwater discharge, *Biogeochemistry*, *63*, 187–205.
- Ullman, W. J., B. Chang, D. C. Miller, and J. A. Madsen (2003), Groundwater mixing, nutrient diagenesis, and discharges across a sandy beach-

- face, Cape Henlopen, Delaware (USA), *Estuarine Coastal Shelf Sci.*, *57*, 539–552.
- Valiela, I., J. Costa, K. Foreman, J. Teal, B. Howes, and D. Aubrey (1990), Groundwater-borne inputs from watersheds to coastal waters, *Biogeochemistry*, *10*, 177–198.
- Valiela, I., et al. (1992), Couplings of watersheds and coastal waters: Sources and consequences of nutrient enrichment in Waquoit Bay, Massachusetts, *Estuaries*, *15*, 443–457.
- Valiela, I., G. Collins, J. Kremer, K. Lajtha, M. Geist, M. Seely, J. Brawley, and C. H. Sham (1997), Nitrogen loading from coastal watersheds to receiving: New method and application, *Ecol. Appl.*, *7*, 358–380.
- Van Cappellen, P., and Y. Wang (1995), Metal cycling in surface sediments: Modeling the interplay of transport and reaction, in *Metal Contaminated Sediments*, edited by H. E. Allen, pp. 21–62, Ann Arbor Press, Chelsea, Mich.
- Vanek, V. (1990), In situ treatment of iron-rich groundwater by addition of nitrate, *Rep.* *33*, Lunds Univ., Lund, Sweden.
- Weiskel, P. K., and B. L. Howes (1991), Dissolved nitrogen flux through a small coastal watershed, *Water Resour. Res.*, *27*, 2929–2939.
- Weiskel, P. K., and B. L. Howes (1992), Differential transport of nitrogen and phosphorus from septic systems through a coastal watershed, *Environ. Sci. Technol.*, *26*, 352–360.
- Wigley, T. M. L., and L. N. Plummer (1976), Mixing of carbonate waters, *Geochim. Cosmochim. Acta*, *40*, 989–995.
- Windom, H. L., W. S. Moore, L. F. H. Niencheski, and R. A. Jahnke (2006), Submarine groundwater discharge: A large, previously unrecognized source of dissolved iron to the South Atlantic Ocean, *Mar. Chem.*, *102*, 252–266.
- Wriedt, G., and M. Rode (2006), Modelling nitrate transport and turnover in a lowland catchment system, *J. Hydrol.*, *328*, 157–176.

C. Meile, Department of Marine Sciences, University of Georgia, Athens, GA 30602-3636, USA.

C. P. Slomp and C. Spiteri, Department of Earth Science–Geochemistry, Faculty of Geosciences, Utrecht University, P.O. Box 80021, NL-3508 TA Utrecht, Netherlands. (c.spiteri@geo.uu.nl)

K. Tuncay, Faculty of Engineering, Middle East Technical University, 06531 Ankara, Turkey.